DEVELOPMENT OF A MICROCHANNEL HEAT SINK FOR THERMAL MANAGEMENT

YEO WEI LONG

MASTER OF ENGINEERING SCIENCE

FACULTYOF ENGINEERING AND GREEN TECHNOLOGY
UNIVERSITI TUNKU ABDUL RAHMAN
JANUARY 2019

DEVELOPMENT OF A MICROCHANNEL HEAT SINK FOR THERMAL MANAGEMENT

By

YEO WEI LONG

A dissertation submitted to the Department of electronic engineering,
Faculty of Engineering and Green Technology,
Universiti Tunku Abdul Rahman,
in partial fulfillment of the requirements for the degree of
Master of Engineering Science
January 2019

ABSTRACT

DEVELOPMENT OF A MICROCHANNEL HEAT SINK FOR THERMAL MANAGEMENT

With the rapid development in the electronic industry, the sizes of majority of the electronic devices (e.g. VLSI systems, LEDs, micro reactors, etc.) have undergone significant reduction. Due to their minute sizes, effective dissipation of the heat accumulated in the electronic chips has become a challenging task, since failing of doing so, may cause reliability issues to the devices. Microchannel heat sink (MCHS) is found to provide the most reliable cooling technology compared to conventional heat sink due to its small size, low coolant requirements and its superior command over heat carrying capability provided by small hydraulic diameter.

Here, MCHSs with extended surface technique were investigated numerically and experimentally in terms of fluid flow and heat transfer characteristics. A three-dimensional MCHS model was drawn and simulated using Ansys Fluent. The simulation and experimental result of MCHS with extended surface was compared to rectangular MCHS. This study focuses on Reynolds number less than 1200 which is in laminar flow. The collected result shows that the extended surface technique enhances the heat transfer performance. The presence of micro-fins helps to disrupt the thermal boundary layer and also increases the pressure drop.

The validation result indicates that the existence of micro-fins significantly enhances the heat transfer performance. The designs of various geometries micro-fins ware introduced and studied in the modelling part. The average wall temperature and Nusselt number are calculated and plotted with respect to the Reynolds number at heat flux equals 100 W/cm^2. The result shows that micro-fins with diverging cylindrical geometry incorporated with triangular ribs (Case E) perform well at Reynolds number less than 700; whereas those incorporated with semi-circle ribs (Case C) are suitable for Reynolds number more than 700.

ACKNOWLEDGEMENT

My utmost gratitude towards my supervisors, Ir. Dr. Yeap Kim Ho and Prof. Ir. Dr. Ong Kok Seng for the time, effort, and immense knowledge contributed throughout my Master study and research. The completion of this dissertation would not have been possible without their guidance. I would like to thank everyone who had contributed to the successful completion of this project.

I am highly indebted and thoroughly grateful to Dr. Lai Koon Chun for his generous guidance, encouragement and support throughout the research.

The project is funded by the University Internal Fund (UTARRF) under project IPSR/RMC/UTARRF/2016-C1/L1.

APPROVAL SHEET

This dissertation entitled "**DEVELOPMENT OF A MICROCHANNEL HEAT SINK FOR THERMAL MANAGEMENT"** was prepared by YEO WEI LONG and submitted as partial fulfillment of the requirements for the degree of Master of Engineering Science at Universiti Tunku Abdul Rahman.

Approved by:

_____
(Ir. Dr. Yeap Kim Ho)

Date:……..
Supervisor
Department of Electronic Engineering
Faculty of Engineering and Green Technology
Universiti Tunku Abdul Rahman

_____
(Prof. Dr. Ir. Ong Kok Seng)

Date:……..
Co-supervisor
Department of Industrial Engineering
Faculty of Engineering and Green Technology
Universiti Tunku Abdul Rahman

FACULTY OF ENGINEERING AND GREEN TECHNOLOGY

UNIVERSITI TUNKU ABDUL RAHMAN

Date: _____

SUBMISSION OF THESIS

It is hereby certified that **YEO WEI LONG** (ID No: **17AGM00645**) has completed this thesis entitled "**DEVELOPMENT OF A MICROCHANNEL HEAT SINK FOR THERMAL MANAGEMENT**" under the supervision of Ir. Dr. Yeap Kim Ho (Supervisor) from the Department of Electronic Engineering, Faculty of Engineering and Green Technology, and Prof. Dr. Ir. Ong Kok Seng (Co-Supervisor) from the Department of Industrial Engineering, Faculty of Engineering and Green Technology.

I understand that the University will upload softcopy of my thesis in pdf format into UTAR Institutional Repository, which may be made accessible to UTAR community and public

Yours truly,

_____

(YEO WEI LONG)

DECLARATION

I, YEO WEI LONG, hereby declare that the dissertation is based on my original work except for quotations and citations which have been duly acknowledged. I also declare that it has not been previously or concurrently submitted for any other degree at UTAR or other institutions.

Name _____

Date _____

TABLE OF CONTENT

LIST OF TABLE

LIST OF FIGURES

LIST OF SYMBOLS AND ABBREVIATIONS

A	cross-sectional area
A_c	contact surface area of water and heat sink
d	hydraulic diameter
f	friction factor
H	height of microchannel
h	heat transfer coefficient
IC	Integrated circuit
K	fluid thermal conductivity
L	length of microchannel
MCHS	Microchannel heat sink
Nu	Nusselt number
Q	total heat transfer
Q_f	flow rate
Re	Reynolds number
T_{in}	inlet temperature
T_{out}	outlet temperature
T_w	wall temperature
u	velocity of fluid
W	width of microchannel
ΔT	temperature difference
μ	viscosity of fluid
ρ	density of fluid

CHAPTER 1

INTRODUCTION

1.1 Background

Thermal management plays an essential role in enabling the technology growth of advanced microelectronic systems. Furthermore, it has expedited the advancement of microelectronic systems, modern computers with high performance and consumer products.

The requirements for integrated circuits (ICs) to have faster speed and more functionalities have led to the miniaturization of the chip. This phenomenon, however, creates a concern on the effective thermal management since a large amount of heat is generated and trapped in a small surface area (Agostini et al., 2007, Ong et al., 2016, Lai et al., 2015). The heat fluxes dissipation levels in the chips are predicted to exceed beyond 100 W/cm^2 in 2020 (Phillips, 1990, Mudawar, 2001, Ross, 2004). For instance, super computers, advanced military equipment, opto-electronic equipment, power devices and electric vehicles are found to contain heat fluxes dissipation of 102 -103 W/cm^2 (Mudawar, 2001).

The performance of electronic systems declines significantly once the temperature threshold limit of the system is exceeded. Moreover, the

properties of the materials used to construct the equipment, such as the structural integrity and chemical stability, are found to have deteriorated as a result of an accumulation of excessive temperature in the device. These factors contribute to the reduction of the life span of the equipment. Hence, thermal management design aims to sustain the temperature distribution throughout the products so that it can be kept below the permissible limit. Because of this reason, thermal management plays an important role to maintain the performance and reliability of the electronic products.

Conventional air cooling methods appear to be insufficient to remove the excess heat from the compact electronic chips and circuits which have limited surface areas (Ong et al., 2017b, Ong et al., 2017c, Ong et al., 2017a). In 2003, the International Technology Roadmap for Semiconductors forecasted that the thermal resistance of the junction-ambient was required to be decreased to 0.18 °C/W before 2010. Hence, it is crucial to develop an efficient cooling method which can perform more effectively than the air-cooling technology. Microchannel heat sinks are one of the popular alternatives to resolve heat dissipation issue in micro-scaled platforms or microchannels. This compact device has drawn considerable attention, attributed to its large surface area-to-volume ratio, heat transfer coefficient with high convective and relatively less demand of coolant inventory.

The concept of microfluidic cooling technology was first established in 1981 by Tuckerman and Pease (1981b). Due to its potential in handling ultra-high heat fluxes, microchannel heat sinks have gained significant attention for

extensive research (Peiyi and Little, 1983, Rahman and Gui, 1993a, Rahman and Gui, 1993b, Peng and Peterson, 1995). The basic working principle of microchannel heat sinks is rather straightforward. The heat produced by the electronic components is transferred by forced convection to the coolant within the multiple microchannel heat sink mounted at the back of the electronic components substrate. The channels with microscopic sizes reduce the thickness of the thermal boundary layer. This allows convective resistance to be minimized and, therefore, provides high cooling rates to the components.

1.2 Problem Statements

There is no doubt that the microchannel heat sink is a good solution for dissipating heat. As the technology node of microelectronic systems continue to shrink, however, the design of its geometrical structure to allow effective heat dissipation has become increasingly challenging. Hence, a higher heat transfer coefficient microchannel heat sink is highly demanded. According to past literature (Sui et al., 2010, Mohammed et al., 2011a, Deng et al., 2015), researches on the design of microchannel heat sink have mostly focused on the optimization of the design. Methods to increase the heat transfer coefficient (such as extending the surface for heat transfer) have not been widely explored. It may therefore be worthwhile to look into this aspect when designing the microchannel heat sink.

1.3 Research Objectives

1. To design and fabricate a microchannel heat sink for effective thermal management.
2. To investigate the effect of the channel design through numerical analysis.
3. To characterize and evaluate the performance of the microchannel heat sink.

1.4 Thesis Organization

In this dissertation, 5 chapters are presented. Chapter 1 introduces the background of the microchannel heat sink. The advantages of the microchannel heat sink in advanced technology, particularly in microelectronic systems are highlighted.

In chapter 2, the related literature is reviewed. The concepts and the design parameters of some existing microchannels as well as the materials for fabricating the heat sink are discussed. The reviews of microchannel heat sink performance are separated into two categories, i.e. numerical analysis and experimental investigation.

Chapter 3 describes the experimental and numerical work in developing the microchannel heat sink. The design method, numerical simulation method and results are revealed in this chapter.

In chapter 4, modification of geometry, simulation results and discussion of the developed microchannel heat sink are reported. The simulation results are validated and compared with the conventional microchannel.

In chapter 5, the research work is concluded in this chapter. The summary based on numerical analysis and experimental results are reported. Future work is proposed so as to improve the device performance.

CHAPTER 2

LITERATURE REVIEW

2.1 Introduction to Microchannel Heat Sink

Since the past decades, the electronic industries have witnessed the miniaturization of electronic components. Most of the electronic devices (i.e. laptops, smart phones, etc.) are required to be small, portable and able to execute tasks at a rapid rate. In order to achieve this goal, integrated circuits (ICs) with high-power have been manufactured. There are billions of transistors that operate at high frequencies in a high-powered integrated circuit. This phenomenon creates a concern on the effective thermal management when a large amount of heat is generated within a limited surface area (Agostini et al., 2007). As shown in Figure 2.1, the complexity of an integrated circuit chip grows at an extraordinarily fast pace. Moreover, Moore's law has predicted that the quantity of transistors contained in an IC would be approximately two times in every 18 months as shown in Figure 2.2 (König and Ostendorf, 2015). This indicates that the amount of heat necessary to be dissipated would increase proportionately. According to Xie et al. (2015), at every increase of 2 ℃ temperature, the reliability of a silicon chip will decline for approximately 10 %. As depicted in Figure 2.3, the primary factor leading to failure in electronic chips is due to excessive high temperature (i.e. 55%). This issue is encountered by the microprocessor chips in personal

computer (PC) today. Generally, forced air convection fans were utilized to cool the chips. However, a standard-cooling method appears to be insufficient to remove the excessive heat, when dealing with electronic devices that work at high frequencies (i.e. in the range of GHz) and involve billions of transistors. To solve this issue, fluids were forced through microchannels manufactured within the electronic devices (Tuckerman and Pease, 1981b).

The studies of microchannel heat sinks have been carried out widely in the recent decade to manage thermal dissipation in electronic systems. Based on their high area-to-volume ratio and their benefits in terms of small and compact size, microchannel heat sinks have become promising candidates for the efficient dissipation of heat in devices, especially integrated circuits chips.

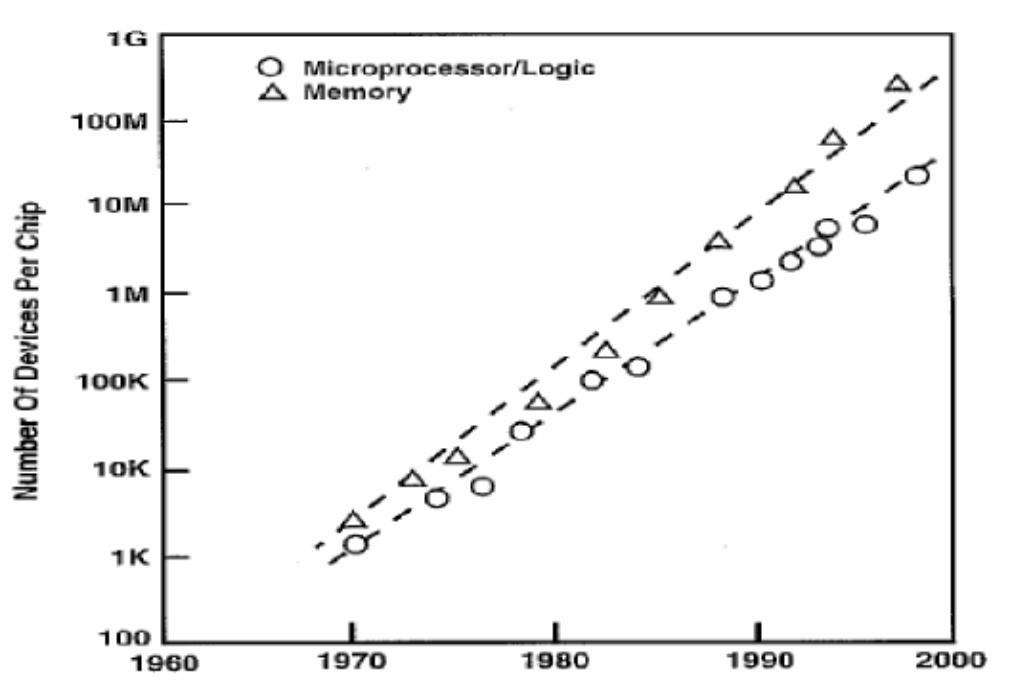

Figure 2.1: Circuit complexity

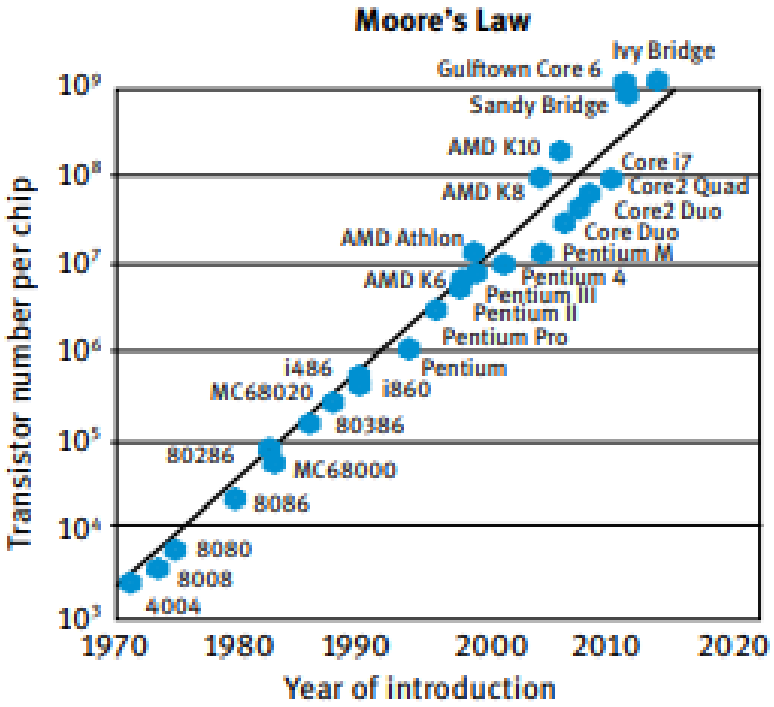

Figure 2.2: Moores' law (König and Ostendorf, 2015)

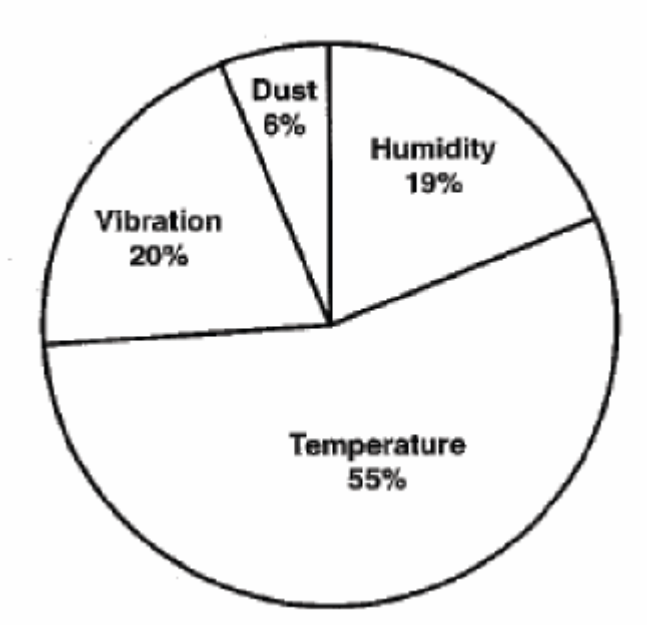

Figure 2.3: Factor for electronic failure

2.2 Heat Transfer

The transfer of heat energy occurs when there is a difference in temperature. As a vector quantity, heat energy moves from one system to another via temperature gradient. Energy cannot be produced or destroyed based on the law of conservation of to energy. Hence, heat energy can only be transferred from one location to another to reach a state of thermal equilibrium. To achieve thermal equilibrium, heat is commonly transferred in three different ways i.e. convection, conduction and radiation.

2.2.1 Heat Transfer by Convection

Heat transfer by convection is considered as the major types of heat transfer in gas and liquid phases. Generally, convection occurs when higher heat energy particles in liquids or gases replace or move to the less heat energy particles. Convection can be classified into two types, i.e. natural convection and forced convection. Forced convection occurs when external devices are applied to force the fluid to flow across the surface. In contrast to forced convection, however, natural convection occurs when the temperature variation in the fluid generates density differences. Buoyancy forces which affect the fluid motion are induced as a result of the differences.

2.2.2 Heat transfer by Conduction

In nature, conduction heat transfer is the most frequently occurred phenomenon. In the conduction process, heat energy is transferred within solid

materials. When two different temperature solid materials are in contact with each other, heat energy transfers from the higher temperature solid to the lower temperature solid and finally a state of thermal equilibrium obtained. At the subatomic level, it can be seen that the particles at the hotter surface gain more energy and move faster. When put in contact with a cooler surface, the hotter particles collide with the cooler and slower particles. As they collide, a fraction of the energy from the fast moving particles passes to the slow moving particles. The process repeats until all the energy is homogeneously distributed among all particles.

2.2.3 Radiation

Unlike the convection and conduction processes, radiation is a heat transfer process which is independent of the relations between the heated object and its heat source. Instead, radiation is caused by the transport of energy which involves electromagnetic waves traveling at the speed of light. Electromagnetic waves radiate out from hot objects in all directions, with a wavelength of 0.75 μm to 1 mm until they penetrate into another medium. This allows heat energy carried by the waves to be either absorbed or reflected.

2.3 Reynolds number

A dimensionless parameter Reynolds number (Re) is utilized to determine the fluid flow form is in laminar or turbulent. Technically, it is highly essential in predicting the flow patterns in a fluid's behaviour by

referring to numerous properties like density of fluid (ρ), viscosity of fluid (μ), velocity (u) and hydraulic diameter (d).Instead of the length, the Re number for open channel flow is calculated based on the hydraulic diameter. Re number and the hydraulic diameter can be expressed using the following equation:

$$\mathrm{Re} = \rho u d / \mu \tag{2.1}$$

$$d = \frac{4A}{P} = \frac{2WH}{W + H} \tag{2.2}$$

where A represents the pipe's cross-sectional area, P represents the wetted perimeter and W and H represent the width and height respectively of the microcahnnel. Table 2.1 shows the types of flow under different Reynolds number.

Table 2.1: Different Reynolds Numbers for different types of flow

Types of flow	Range of Reynolds Number
Laminar flow	Re ≤ 2300
Transition flow	2300 < Re < 4000
Turbulent flow	Re > 4000

2.4 Nusselt number

Nusselt number (Nu) is a dimensionless parameter which is defined as the ratio of convective to conductive heat transfer across the surface. It provides a measure of heat transfer enhancement or convection heat transfer occurring at the surface. The larger number is the Nusselt number the more

effective is the convection process. Nusselt number (Nu) is expressed in (2.3) and (2.4) below:

$$\frac{qconv}{qcond} = \frac{h\Delta T}{k\frac{\Delta T}{L}} = \frac{hL}{K} = Nu \tag{2.3}$$

$$h = \frac{Q}{NA_c\Delta T} \tag{2.4}$$

where A_c represents the water and heat sink contact surface area, K represents the thermal conductivity of the fluid, the total heat transfer was represented by Q, and h was to represents the heat transfer coefficient. From (2.4), it can be seen that h is inversely proportional to temperature difference (ΔT). ΔT can be expressed as $\Delta T = Tw - (Tin + Tout) / 2$, where T_w, T_{in}, T_{out} represent the wall temperature, inlet temperature and outlet temperature respectively. From the relationship of h and ΔT, a smaller temperature difference can increase the value of h, resulting in a larger value of Nu. When Nusselt number is close to 1, the heat transfer across the layer is purely conduction.

2.5 Overall thermal performance

The overall performance of a microchannel heat sink can be evaluated based on the overall thermal performance factor. As declared in the preceding section, a large number of Nusselt number is necessary for a more effective convection. However, the thermal performance of a microchannel also depends on several factors like friction factor and pressure drops. According to Shen et al.(2018) and Li et al.(2014), the overall thermal performance can be written as:

$$\eta = \frac{Nu / Nu_0}{\left(\Delta f / \Delta f_0\right)^{1/3}}, \; f = P / \mathrm{Re} \tag{2.5}$$

where f represents the friction factor which is identify as the ratio of the pressure to Reynolds number. The relationship among Nusselt number, pressure drop and Reynolds number are useful when assessing the overall performance, it brings equilibrium to surface temperature and pressure drop. Both temperature and pressure drop are compared with those obtained from bare rectangular microchannel.

2.6 Microchannel Heat Sinks

In the 1980s, the first silicon microchannels heat sink was successfully developed using standard semiconductor fabrication techniques. According to Tuckerman and Pease (1981b), the silicon microchannels dissipate undesired heat from an electronic chip by utilizing water as the working fluid. The 1 cm^2 microchannels were etched in a silicon substrate. The design's channel width was roughly 60 μm along with the channel height fluctuates among 287 μm and 376 μm. The microchannel was successful in maintaining the chip temperature below 110 ℃ by effectively dissipating heat up to 790 W/cm^2. The small space occupied by the silicon microchannels has attracted significant attention from the scientific community and it has led to extensive investigation of the possibility of new transport physics.

After the pioneering effort of Tuckerman and Pease, Peiyi and Little (1983) utilized gas flow to evaluate experimentally the effectiveness of fluid

flow in microchannels. The determined friction factors presented in laminar regime were observed to be higher than expected. The transition of Reynolds number concluded in their report ranges from 350 to 900. In 1994, the transition period from laminar-to turbulent in microchannels has been evaluated experimentally by Peng and his colleagues (Peng et al., 1994). The Reynolds numbers in this experiment were found to be lower than that expected based on the conventional theory. In another experiment conducted in 1995, disparities again were found between the conventional flow theory and the experimental results for microchannels (Peng and Peterson, 1995). For hydraulic diameters in microchannel which range between 133 μm to 367 μm, the friction factor is found to depend on the channel aspect ratio and hydraulic diameter.

Judy et al. (2002) conducted an experiment on both square and round cross section microchannels to test the pressure drop with hydraulic diameters that ranged from 15 to 150 μm. Methanol, Isopropanol and DI water have been tested over the Reynolds number in the range from 8 to 2300. For each of these cases, the laminar flow showed no distinguishable deviation. Liu and Garimella (2004) experimentally tested the pressure drop analysis and flow visualization for microchannels with 244 to 974 μm of hydraulic diameters through a range of 230 to 6500 Reynolds number. Comparisons between the measured results and numerical calculations for the pressure drop were carried out. To achieve the overall average relation between the Reynolds number (Re) and Nusselt (Nu) number for certain geometry of the heat sink, the calculations were carried out for different overall pressure drops within the

channel. In fact, Choi (1991) who performed studies regarding to microchannels consists of diameters ranging between 3 to 8 μm, declared that the Nusselt number depends on the Reynolds number within laminar microchannel flow as well.

In Tuckerman and Pease (1981b), the development of microscale heat sinks was discussed. It was concluded in the report that the micochannels were to maintain a typical pressure drop of more than two bars. Also, a high surface temperature was undesirable from the perspective of reliability and performance.

The idea of developing a manifold microchannel heat sink was originally presented by Lee and Garimella (2006). The heat sink consisted of more inlet and outlet manifolds as compared to the conventional microchannel heat sinks and these manifolds alternate along the microchannel's length at a periodic distance. Due to this geometrical structure, the coolant flowed towards the manifolds from the inlet and formed separate streams. Each of the stream flowed through a short section of microchannels, allowing the laminar to flow at a constant rate. As compared to conventional microchannel heat sink, the pressure drops obtained were lower, according to a factor which is equivalent to the number of outlet or inlet of the manifold. The drawbacks of this structure are the low heat transfer efficiency at the region underneath the manifolds.

The study performed by Bavière et al. (2006) indicates that by varying

the cross-sectional dimensions of the microchannel, the temperature gradient and the maximum temperature can be further reduced. However, this method can cause a sudden increase in the pressure drop. This may result in acceleration on the fluid flow velocity which could, therefore, deteriorate the efficiency of the heat sink.

A numerical study was performed by Rahman and Gui (1993b) to evaluate the forced convection heat transfer in microchannel heat sinks. In this study, a simplified 3D conjugate heat transfer model was built (i.e. 3D heat transfer and 2D fluid flow). In their study, the temperature dependent thermos physical property technique has been applied to evaluate the heat transfer's result. The heat flow is investigated by varying the channel's geometry and the fluid's thermos physical properties. They concluded that the different ways of defining the Nusselt number may lead to different results even if the same experiment data was used.

In the past decades, the single or two-phase flow mechanisms analyses have been widely studied by the microchannel heat sink researches. In Rahman and Gui (1993a), thermal performance comparisons on the multi-layer and single layer microchannel heat sink were performed. It was found that multi-stack microchannel heat sinks reduce the temperature gradient dramatically as compared to single-layered micro channel. The result is corroborated by the experiment conducted by (Gui and Scaringe, 1995). In the multi-stack microchannel structure, the pressure drops in direct proportional with the number of layers when the flow rate is uniform. It is worthwhile

noting that, the multi-stacked microchannel heat sink thermal performance is also influenced by the thermal conductivity, flow rate and the channel aspect ratio of the base material. The typical rectangular cross section parallel flow microchannel heat sink with single layer and multi-layer are shown in Figures 2.4 and 2.5 respectively.

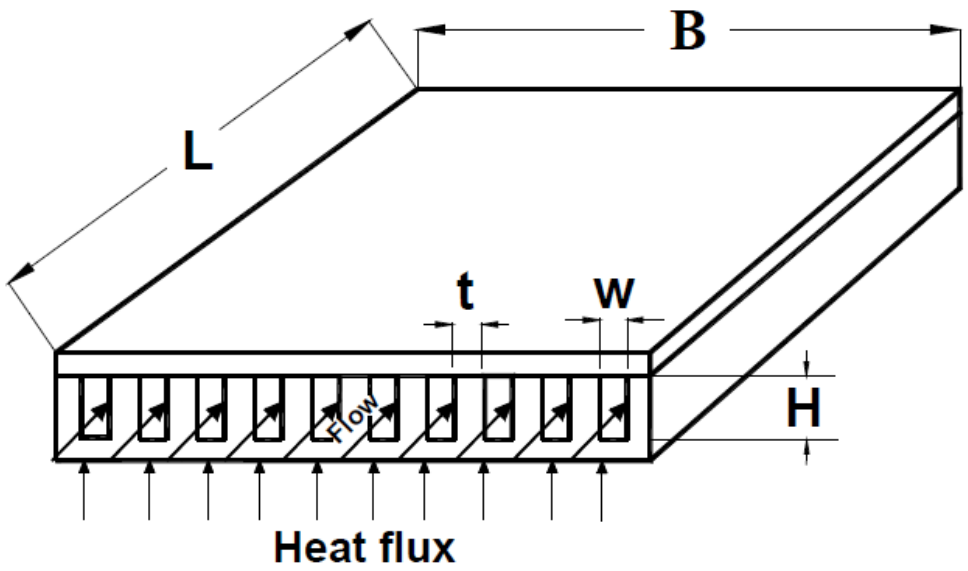

Figure 2.4: Typical rectangular cross section parallel flow single layer microchannel heat sink

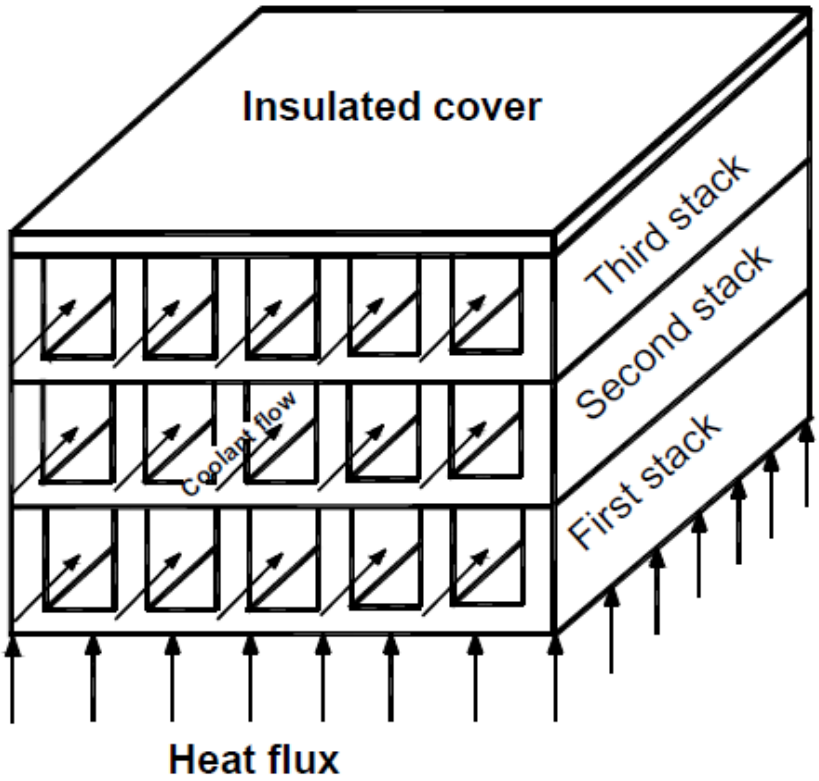

Figure 2.5: Typical rectangular cross section parallel flow multi-layer microchannel heat sink

2.6.1 Analyses on Single-Phase Flow Microchannel Heat Sink

Microchannel heat sinks with single phase and two phases flow have been widely exploited in the past decades. Analyses on these microchannel heat sinks are essential so as to develop a more effective heat sink in this project. Thus, in this and the flowing subsections, the single-phase flow and two phase flow microchannel heat sink will be discussed in detail.

Harms et al. (1999) presented a single phase flow rectangular microchannels with width, w= 251 μm and height, H = 1000 μm. In their

report, working fluid was chosen as deionized DI water. The experiment result indicated that the correlation proposed by Shah and London (1978) for laminar flow was able to accurately predict the Nusselt number. The authors also highlighted in their report that the performance of the laminar flow better than turbulent flow of the microchannel developed in terms of heat transfer characteristics and flow.

Qu and Mudawar (2002b) presented the heat transfer characteristics and pressure drop in a rectangular microchannels heat sink with single phase flow (w = 231 μm, H = 713 μm) which was made of copper. The coolant of the microchannel heat sink was deionized DI water. SIMPLE algorithm was applied to solve the governing continuity, momentum and energy equations (Patankar, 1980). It was observed that the maximum temperature generally occurred at the microchannel's base surface for any distance longitudinal to the length of the microchannel. The lowest temperature, on the other hand, was formed at the parts filled with deionized DI water. Besides, early transitions from laminar to turbulent flow were observed within the microchannels.

Rectangular cross sectional microchannel heat sinks with single and double layer counter flow was reported by Chong et al. (2002). The modeling was done by applying the thermal resistance network method. The results obtained were in good agreement with the results obtained by the FLUENT commercial software. By utilizing the multivariable constrained direct search method, the optimized dimensions of the microchannel were obtained (Box,

1965). The optimized single and double layers counter flow microchannel developed for laminar flow were found to have outperformed those developed for turbulent flow in both thermally and hydro-dynamically conditions. This, however, comes with the expense of high pressure drops of 1.2 bars and a high channel aspect ratio of 10. It is worthwhile noting that the temperature distribution, heat flux and flow with non-uniformities were not considered in the report.

Wei and Joshi (2004) presented the analysis of stacked parallel flow arrangement silicon microchannel heat sinks. In their report, iterative resistance network with one dimension was utilized to determine the heat sink's thermal resistance. Experimental tests for the proposed microchannel heat sinks were carried out in flow distributions with uniform pressure drop, pumping power, and flow rate, as well as, steady heat flux. The single stack heat sink's thermal resistances were normalized. They reported that the effectiveness of stacked structures depended on thermal conductivities of the material. A high conductivity material could improve the thermal performance, but at low flow rate, the main thermal resistance existed on the fluid side. However, the microchannel heat sink's temperature distribution is not presented.

Li et al. (2004) evaluated numerically the heat transfer of microchannel heat sink with 57 μm width and 180 μm height made up of silicon utilizing 3D conjugate heat transfer model. The governing equations were solved by the Tri-Diagonal Matrix Algorithm with the finite difference

numerical code. The results obtained indicated that the liquid's thermophysical properties could considerably affect the flow and heat transfer within the microchannel heat sink. Moreover, to compute the overall average Nu number for the microchannel heat sink, they proposed a correlation could be adopted.

Lee et al. (2005) evaluated experimentally the rectangular copper microchannels (w = 194 to 534 μm, Ar = 5) thermal behavior with single phase flow. DI water was chosen as the working fluid. FLUENT was used to carry out numerical simulation to anticipate the flow Nu number. The acquired experimental results were in close agreement with the numerical results.

Zhang et al. (2004) and Zhang et al. (2005) have performed a study on flip chip ball grid array packages liquid cooling for microchannel heat sinks with a width of 210 μm. An aspect ratio (Ar) of 10 made up of aluminum with single stack was analyzed. In their study, the microchannel heat sinks were mounted onto two different chips with dimensions of 10 x 10 mm^2 and 12 x 12 mm^2. The microchannel heat sink's thermal resistances at different coolant flow rates were numerically determined utilizing the thermal resistance network. The calculated thermal resistances for water cooling in 10 x 10 mm^2 and 12 x 12 mm^2 chips ranged from 0.59 to 0.44 ℃/W and 0.44 to 0.32 ℃/W respectively.

Shah and London (1978) presented a review on the different methods adopted to determine the heat transfer coefficients and the pressure drop of single-phase laminar flow. Moreover, those modified methods have also been

utilized for microchannel heat sinks by some researchers (Zhang et al., 2005, Chong et al., 2002, Qu and Mudawar, 2002b, Wei and Joshi, 2004). In the last decade, single phase flow in microchannel heat sinks have been widely implemented due to its non-complexity and high efficiency as compared to two phase flow microchannel.

2.6.2 Two-Phase Flow Microchannel Heat Sink Analysis

Microchannel heat sinks in two-phase flow studies are relatively new and its potential applications in high flux electronics cooling have drawn the attention of researchers working in this field. The fundamental heat transfer characteristics and flow type are generally investigated in microchannel heat sinks in two-phase flow. Currently, numerical simulation analyses for two-phase flow microchannel heat sinks with performance are rare in the literature.

Flow boiling experiments in diameter less than 3 mm small tubes were firstly performed by Bergles and Dormer Jr (1969). The pressure drop related to water flow boiling in length to diameter ratio of 24 to 195 and diameters from 1.57 to 5.03 mm horizontal tubes was the primary investigation of their research. The velocity of the liquid, inlet temperature and wall heat fluxes were changed from 1.51 to 18.2 m/s, 10 to 62.7 ℃ and 0 to 1733.6 W/cm^2 respectively. The outcomes of the experiment indicated that once the water started to boil, the pressure increased rapidly for a given inlet temperature and velocity.

By conducting 24 experimental investigations on 10 different types of fluids, a general correlation was developed by Kandlikar (1990) for boiling heat transfer with two-phase flow at the saturate point and within the vertical and horizontal tubes. A mean deviation of 15.9% for all the data was obtained. In his later works in Kandlikar and Steinke (2002), Kandlikar and Balasubramanian (2003), the correlation was initially introduced for macro-sized tubes. However, Kandlikar and his research team have customized the correlation in order to accommodate microchannels in two-phase flow.

Wambsganss et al. (1993) reported an experimental investigation on the flow boiling in a small circular tube with refrigerant R113. The experimental result showed that by fixing all other parameters the heat transfer coefficient with two-phase (h_{tp}) rose with the growing of heat flux (q), this is to say that, flow boiling heat transfer coefficient is weakly dependent on mass flux (G) and highly dependent on the applied heat flux. The experiment also indicated that the heat transfer's dominant mode within the quality vary from 0 to 0.9 was the nucleate boiling.

Bowers and Mudawar carried out the boiling flow tests with R113 flowing through the hydraulic tubes of diameters 0.510 and 2.54 mm and in a multiport circular channels (Bowers and Mudawar, 1994b, Bowers and Mudawar, 1994c, Bowers and Mudawar, 1994a). These experiments developed an effective method to obtain high heat fluxes by boiling in narrow channels, coupled with low pressure drops and flow rates.

A study on boiling heat transfer in a horizontal rectangular channel with D_h of 2.40 mm was conducted by Tran et al. (1996). The authors discovered that nucleate boiling was the dominant heat transfer mechanism. For low vapor qualities which were less than 0.3, two-phase heat transfer coefficient (h_{tp}) was observed to be reduced when vapor quality increases. The empirical correlation presented in this report indicated that h_{tp} was a function of the Weber number, liquid-vapor density ratio and boiling number.

Zhang et al. (2002) presented a report which analysed the flow boiling tests of the two phase flow single-channel and multi-channel (hydraulic diameter <100 μm) heat sinks. The heat balance equations for heat sink developed in this report were solved by employing the Finite Volume Method (FVM) (Patankar, 1980). To determine the boiling heat transfer with two phase flow, the correlation developed by Kandlikar (1990) was also applied. The homogenous flow was assumed to model the pressure drop. The external correlation developed by Stanley et al. (1997) was utilized to obtain the two-phase friction coefficient. The simulation results in the report showed close agreement with the measured results.

Apart from the single phase flow, Qu and Mudawar have also conducted an experiment to evaluate the water flow boiling in a 231 x 713 μm^2 cross section rectangular microchannels (Qu and Mudawar, 2003a, Qu and Mudawar, 2003b). In Qu and Mudawar (2003a), various empirical correlations for heat transfer coefficient with two-phase flow microchannels have been studied. In Qu and Mudawar (2003b), the empirical correlations to

predict the rectangular microchannels with two-phase flow pressure drops have been studied. Qu and Mudawar concluded that merely the correlation introduced by Mishima and Hibiki (1996) accurately predicted the pressure drops with an error margin of about 13 %. At the end of the experiments, this reports presented a new correlation to estimate the pressure drops in microchannels with two-phase flow. The correlation is summarized in Table 2.2.

Table 2.2: Correlations given by different researches for empirical constant C

Reference	Correlation for the empirical constant C
Conventional Lockhart-Martinelli	$C = 5$ for laminar flow
(Mishima and Hibiki, 1996)	$C = 21(1 - e^{-0.319 \times 10^3 D_h})$
(Lee and Lee, 2001)	$C = A\lambda^a \psi^r Re^s{}_{LO}$ Ψ, λ is the dimensionless, *s, r and a* represent constants can be found in the literature and Re_{Lo} represent the Re number of liquid only Reynolds number.
(Qu and Mudawar, 2003b)	$C = 21\left(1 - e^{-0.319 \times 10^3 D_h}\right)(0.00418G + 0.0613)$ G is the mass flux of the coolant.

In Kandlikar and Balasubramanian(2003) and Kandlikar and Balasubramanian (2004), the flow boiling heat transfer in microchannels was predicted using the modified Kandlikar correlation. The outcomes of the prediction were compared with existing experimental results and were found to be in agreement. As encountered in most microchannels, the flow boiling in low Reynolds number range was observed to be the dominant mechanism for nucleate boiling.

Steinke and Kandlikar (2004) presented an experimental analysis for water flow boiling in six horizontal and parallel microchannels (diameter = 207mm). The outcome of the experimental analysis was found to agree closely to the nucleate boiling dominant regime of the flow boiling correlation developed in (Kandlikar and Balasubramanian, 2004). The results further corroborate the validity of the modified Kandlikar correlation.

As can be seen in Table 2.1, the correlation found in most of the literatures which analyze the two phase flow microchannels are based on modifying the constant C proposed in the Lockhart-Martinelli's correlation (Kawahara et al., 2002). Although the two phase flow microchannel provides prospective performance in high flux electronic cooling, the design comes with the expense of high geometrical complexity and high cost.

2.6.3 Working Principle of the Microchannel Heat Sinks

Generally, the working principle of microchannel heat sinks is rather straightforward. At the back of an IC chip substrate, multiple microchannels are usually machined onto it. The undesired heat energy generated from the electronic component is transferred to the coolant via forced convection. The channels with micro-size lead to a reduction in the thermal boundary layer thickness. This results in a reduction in the convective resistance, allowing heat to be dissipated at an effective rate.

Fluid which is forced to flow through a greater number of small

channels increases the level of heat transfer from the hot source, such as bulbs, ICs, etc. to the flowing fluid. The number of channels for small hydraulic diameter is more when compared to larger diameter channels, and hence, the overall thermal performance of heat sink with smallest hydraulic diameter is better (Lin et al., 2018). As mentioned in chapter 1, microchannels were first proposed by Tuckerman and Pease in 1981 to dissipate heat in electronic components. Their pioneering work was well received by the electronics community, and it has led to an extensive investigation on different characteristics of microchannels for electronic cooling applications (Husain and Kim, 2008, Mohammed et al., 2011b).

Theoretical concepts of energy and heat transfer are the underlying requirement to understand water convection (Siddheshwar and Veena, 2018). Heat transfer is the energy in transit caused by a varying temperature. Convection, conduction, radiation, condensation and boiling were the few modes of heat transfer. Generally, convection is the primary heat transfer mode in a microchannel heat sink experiment. Convection is the transfer of heat from a region with higher temperature to that with lower temperature in either fluid (e.g. water) or gas (e.g. air) phase. For convective heat transfer, q stands for heat flux (W/cm^2).

In single phase flow, the convective heat flux can be calculated by monitoring the mass flow rate and the difference of temperature between the outlet and inlet of the liquid contained in the cooling system as depicted in the following equation (Kalteh et al., 2012):

$$q = mC_p(T_{out} - T_{in}) \tag{2.6}$$

where m is mass flow rate, C_p is specific heat at constant pressure and T_{out}, T_{in} represent the inlet and outlet temperature. Equation (2.6) is fundamentally used to interpret the obtained data and to extract essential information met of it.

The heat transfer coefficient h related to the definition of Nusselt number, Nu, can be written as follows (Sahar et al., 2017):

$$h = \frac{K_f N_u}{D_h} \tag{2.7}$$

where K_f represents the fluid thermal conductivity and D_h is the hydraulic diameter. From equation (2.7), it can be observed that the heat transfer coefficient, h, is inversely proportional to the hydraulic diameter, D_h and directly proportional to Nu. Hence, in small hydraulic diameter case, the flow should be laminar and fully developed. The Nusselt number is constant for a fully developed laminar flow in a square channel with constant wall temperature or heat flux. Assuming conventional channel flow, a low *v*alue of D_h increases the heat transfer coefficient h. A high h, nevertheless, results in high Nu and might raise the pressure in the microchannels. Assuming laminar flow, the pressure drop equation can written as (Liu and Garimella, 2004):

$$\Delta P = \frac{K}{D_h{}^2} \times G \tag{2.8}$$

where *K* represents the coefficient and *G* is the volumetric flow rate. Equation (2.8) indicates that the relationship between the pressure drop and hydraulic diameter is inversely proportional. This is to say that, by reducing the hydraulic diameter, the pressure drop will increase and vice versa.

2.6.4 Governing Equations

To analyze the microchannel heat sink with the entire domain, derivation of the the governing equations that involve continuity, momentum and energy from the fundamental principle of fluid flow and heat are necessary to be established. Generally, the governing equations are solved with the following assumptions made when the heat flows through the microchannels (Gunnasegaran et al., 2012, Qu and Mudawar, 2002a):

1. Steady-state for both heat transfer and fluid flow.
2. Incompressible fluid
3. The flow is laminar.
4. Heat sink material and fluid properties are temperature-independent.
5. Ignorable radiation heat transfer.

The dimensionless form of the governing equations for heated microchannel heat sink can be evaluated as (Patankar, 1980):

Continuity

$$\frac{\partial U}{\partial X}+\frac{\partial V}{\partial Y}+\frac{\partial W}{\partial Z}=0 \tag{2.9}$$

Momentum

X-momentum:

$$U\frac{\partial U}{\partial X}+V\frac{\partial U}{\partial Y}+W\frac{\partial U}{\partial Z}=-\frac{d\hat{P}}{dX}+\frac{1}{Re}\left(\frac{\partial^2 U}{\partial X^2}+\frac{\partial^2 U}{\partial Y^2}+\frac{\partial^2 U}{\partial Z^2}\right) \quad (2.10)$$

Y-momentum:

$$U\frac{\partial V}{\partial X}+V\frac{\partial V}{\partial Y}+W\frac{\partial V}{\partial Y}=-\frac{d\hat{P}}{dX}+\frac{1}{Re}\left(\frac{\partial^2 V}{\partial X^2}+\frac{\partial^2 V}{\partial Y^2}+\frac{\partial^2 V}{\partial Z^2}\right) \quad (2.11)$$

Z-momentum:

$$U\frac{\partial W}{\partial X}+V\frac{\partial W}{\partial Y}+W\frac{\partial W}{\partial Y}=-\frac{d\hat{P}}{dZ}+\frac{1}{Re}\left(\frac{\partial^2 W}{\partial X^2}+\frac{\partial^2 W}{\partial Y^2}+\frac{\partial^2 W}{\partial Z^2}\right) \quad (2.12)$$

Energy

$$U\frac{\partial \theta}{\partial X}+V\frac{\partial \theta}{\partial Y}+W\frac{\partial \theta}{\partial Y}=\frac{1}{Re.Pr}\left(\frac{\partial^2 \theta}{\partial X^2}+\frac{\partial^2 \theta}{\partial Y^2}+\frac{\partial^2 \theta}{\partial Z^2}\right) \quad (2.13)$$

where

$$X=\frac{x}{D_h} \quad (2.14)$$

$$Y=\frac{y}{D_h} \quad (2.15)$$

$$Z=\frac{z}{D_h} \quad (2.16)$$

$$U=\frac{u}{u_{in}} \quad (2.17)$$

$$V=\frac{v}{u_{in}} \quad (2.18)$$

$$W=\frac{w}{u_{in}} \quad (2.19)$$

$$\hat{P}=\frac{\Delta P}{\rho u^2{}_{in}} \quad (2.20)$$

represents the dimensionless pressure, and

$$\theta = \frac{T_f - T_i}{T_\omega - T_i} \tag{2.21}$$

represents the dimensionless temperature. Given the complexity of these equations, solving them using computational methods are necessary. Furthermore, the boundary conditions need to be specified for certain particular design (Gunnasegaran et al., 2012). Anyway, the complex approach to solve those equations can be done easily using well-established commercial numerical solver such as Fluent, Comsol etc. The numerical studies will be discussed in the following section.

2.7 Numerical Analysis

The numerical solver codes provide a good start to more complex fluid flow and heat transfer issues. Based on this feature, numerical analysis of the microchannel heat sink in recent years has gained significant interest. The introduction of the numerical simulation tools and the numerical studies of published literatures are further explained in the subsequent section.

2.7.1 Introduction to Numerical Simulation Tools

Traditionally, resistance model was the method used to model the microchannel heat sink (Phillips, 1987). However, this one dimensional modeling method imposes limitation for more complex applications. An

example of which is its inability to solve for flow and heat flux non-uniformities. The resistance model has also been proven to be inappropriate for microchannel heat sinks with two phase flow modeling as well (HEGDE, 2006). Computational fluid dynamics (CFD) is an analysis method that is iterative and computationally intensive, and thus, CFD is a promising solution for more complex applications (Yin et al., 2013, Abubakar and Sidik, 2015, Ramos-Alvarado et al., 2011). In fluid mechanics, CFD is one of the branches that utilize algorithms and numerical methods to analyze and solve issues related to fluid flows. ANSYS FLUENT is a CFD software that is well established for modeling heat transfer, turbulence, flow and reactions for industrial applications (Ghale et al., 2015). This software offers the adaptability to alteration of thermo physical properties with regarding to the effect of temperature. The Navier-Stokes equations act as the background engine which drive the CFD tool to compute fluid flow in single phase (Anderson, 1992). To solve these equations, numerical discretization methods such as finite volume method (FVM) are run in the CFD (Gunnasegaran et al., 2012). FVM is a computational method which generates a converged solution in an iterative manner.

2.7.2 Research Works based on Numerical Analysis

The design and development of microchannel heat sink are generally performed using numerical simulation tools first and validated further via experimental measurement. Over the years, the contribution of the researchers can be mainly divided into two areas: numerical investigation (Hatami and

Ganji, 2014, Rahimi-Gorji et al., 2015, Xie et al., 2014, Leng et al., 2016, Chai et al., 2016) and experimental investigation (do Nascimento et al., 2013, Lee et al., 2005). In this sub-section, the review of numerical analysis by other literature will be discussed.

Li and Olsen (2006a) conducted an investigation to validate the numerical results with the obtained experimental data. In the experiment, the chip and the air inlet velocity were heated to 353 K and 293 K respectively. It was observed that the inlet velocities varied from 1 to 7 m/s. Different turbulence models have been investigated in their work. By assuming both uniform and fully developed conditions, the changes on the heat transfer rate influenced by the channel inlet flow were determined. The reported results indicated that the local heat transfer coefficient with complex distribution occurred on the substrate. Vortex formation and flow separation were also observed in the results. The flow structure obtained from the simulation was in close agreement with the experimental data. The predicted turbulence intensity on the other hand, did not tally with the experimental results. Turbulence treatment is essential at the vicinity of the wall. In the simulation, however, the function of the wall was not appropriately defined.

Wu and Cheng (2003) and Kohl at al. (2005) performed a 3D numerical heat transfer analysis for the rectangular microchannel heat sinks with water as the coolant. The dimensions of the microchannels were 57 μm wide and 180 μm deep. The thickness of the wall separation was 43 μm. To solve the governing equations, the SIMPLE tool that runs on finite difference

method was used. The results showed that in the solid and fluid regions, the temperature increased linearly in proportion to the flow direction. The peak temperature occurred above the channel outlet of the heated heat sink base surface. At around the channel inlet, the Nusselt number and heat flux showed higher values and fluctuated around the channel periphery. Also, zero Nusselt number and heat flux occurred at the corners. A relatively high Re number of 1400 was obtained. In order to reduce the temperature at the base surface of the heated heat sink and around the channel outlet, the solid substrate thermal conductivity was proposed to be increased.

Hong and Cheng (2009) numerically studied fluid flow and heat transfer characteristics in offset strip-fin microchannels. They proposed different size of strip-fin and demonstrated the deformation of boundary layer to enhance the heat transfer. It was found in their work that when the ratio of fin interval to fin length (K) was equal to 1, the optimal value can be obtained. Tokit et al. (2012) proposed the design of an interrupted microchannel heat sink structure. The Nusselt number obtained in their design is higher than conventional microchannel heat sink. Their proposed design also showed higher pressure drop compared to the smooth channel.

Sui et al. (2010) numerically studied the fluid flow and heat transfer in a three-dimensional wavy microchannel with rectangular cross section. They reported that the wavy microchannel showed better heat transfer performance as compared to the rectangular channel with the same cross section. Mohammed et al. (2011a) carried out a numerical simulation to study the

effect of various geometry structures of the channels. They performed a comparative study among three different channel structures namely zigzag, curvy, and step microchannel with straight and wavy microchannel. From the result they collected, the zigzag microchannel heat sink (MCHS) stored the lowest temperature and it had the greatest heat transfer coefficient. They attributed the effective heat transfer results to the presence of the eddy, and recirculation flows around the bending corners. All channels, despite their geometrical structures, were however, found to have higher pressure drop penalty compared to straight microchannel.

Deng et al. (2015) studied the thermal enhancement in re-entrant copper MCHSs. They concluded that the re-entrant microchannel performed better compared to its rectangular channel counterpart due to a wider heat transfer surface. This is to say that, the Ω shape re-entrant channel provided larger heat transfer surface than the rectangular channel. Wang et al. (2015) proposed several shapes of micro-ribs and fabricated the micro-ribs using MEMS process. Their result indicated that the turbulent flow created by the micro-ribs can augment the heat transfer performance. As a trade-off, the pressure drop of the channels also increased.

2.8 Experimental Analysis

An experiment to determine the effect of altitude on electronic cooling has been carried out by Li and Olsen (2006b). The change of altitude would affect the material properties of air due to the deviation of temperature and

atmospheric pressure. The variation could have negative impact on the heat transfer effectiveness, and it may therefore generate higher temperature as compared to cooling device at sea level conditions. In the experiment, a PCB board that involved the heated rectangular blocks mounted in small wind tunnel is investigated in a hypobaric chamber. The variation of the altitude was above sea level within the range of 0 to 5000 m and the variation of air speed was in the range of 1-5 m/s. It can be observed that the thermal wake function and the local adiabatic heat transfer declined with altitude. The experiment provides essential information for large range altitudes and air speed which could be easily found at forced air convection cooling applications.

Mala and Li (1999) conducted an experiment to determine the pressure drop and flow rates to analyze the flow characteristics. The experiments were conducted by using a microtubes ranging from 54 to 254 μm with water flow through it. Significant departure of flow characteristics anticipated by the conventional theory for smaller diameter microtubes has been shown in this report. In large diameters, the experimental outcomes indicated a rough agreement with the conventional theory. Moreover, in lower Reynolds number the measured pressure drop showed close agreement with the value anticipated by the Poiseuille flow theory. The pressure gradient, on the other hand, increased which was against the result predicted by the theory when Reynolds number increases. Thus, the friction factor obtained was higher in comparison to conventional theory. In addition, this paper has also reported a higher pressure gradient shown in fused silica microtubes as compared to stainless

steel microtube. This result indicated that the flow behavior was dependent on the types of the materials used. They concluded that the high pressure gradient might be caused by the surface roughness or the earlier transmission of laminar to turbulent flow.

An experiment has been carried out by Guo and Li (2003) to examine a heated square cylinder heat dissipation in a channel through oscillating flow. The oscillating amplitude and input power were set as constant for the whole experiment. The heat transfer enhancement was investigated based on the Reynolds number (Re) defined from the oscillating frequency and the mean flow velocity. In each oscillating condition, the time averaged Strouhal number and Nusselt number were examined. The "lock-on phenomenon" was performed and reported for the case of a square cylinder. The experimental result of the heat transfer from the square cylinder was significantly optimized, when the lock-on phenomenon occurred at the pulsating frequency. This study indicates that the heat transfer can be optimized by increasing the Reynolds number.

Using liquid crystal thermography, Tu and Hrnjak (2003) carried out an experiment to examine the rectangular duct which relied on forced convection with air for continuous, one-dimensional kernel function. The kernel functions presented by the researchers demonstrated that when the increase of severe non-uniform surface temperature exceeded the inlet temperature generated by the arbitrary heat flux distribution, the outcome of the experiment would turn out to be uncertain. They concluded that the

anticipation of the presented kernel functions were more reliable than the anticipation from the constant heat flux boundary conditions from conventional heat transfer coefficient and the turbulent flow between parallel plates from analytically derived kernel function.

Liu et al. (2011) experimentally investigated the structure of heat sinks with offset strip fins and longitudinal vortex generators (LGVs). The Reynolds number reported in the report is in the range of 170 to 1200, with aspect ratio of 0.067. A hydraulic diameter of 187.5 μm for LGVs with various angles of attack and number of pairs was used. They found that the proposed method could enhance the heat transfer performance by adding the LGVs to enhance the heat transfer performance at the critical range of Reynolds number (600-730). The LVGs of the proposed method is that it tends to generate a high pressure drop.

2.9 Concluding Remarks

The development and concept of the microchannel heat sink have been studied. Owing to its high flux cooling, microchannel heat sinks have been extensively used to dissipate heat in electronic devices. Two-phase flow microchannel heat sinks provide a promising efficient cooling effect when dealing in certain applications which produce high heat flux. However, the design and fabrication process of the heat sinks are complicated and the cost of fabrication is high. Because of these reasons, many researchers diverted their research focus to the design of single phase flow microchannel heat sinks.

The development of the single phase microchannel heat sinks can be mainly divided into two areas i.e. the numerically and experimentally analyses. Based on the information found in the literatures, it was found that most of the researches focused on the geometry optimization of the channel. Enhancement techniques used to extend the surface of heat transfer are yet to be widely explored. Since they produced positive result on high heat flux cooling applications (Jia et al., 2018), it is worthwhile looking into the development of microchannel heat sinks based on the extended surface heat transfer methods.

CHAPTER 3

ANALYSIS OF A MICROCAHNNEL HEAT SINK WITH MICO-FINS

3.1 Introduction

The design and development of a novel microchannel heat sink with extended surface heat transfer enhancement technique is illustrated in this chapter. The structure of the microchannel heat sink shall be outlined and the design shall be theoretically analysed. To show its more superior performance in dissipating heat, the microchannel heat sink (MCHS) with micro-fins is first experimentally compared with their conventional counterparts. Here, we compare a conventional rectangular microchannel heat sink with those which consist of different geometries of micro-fins. Water is selected as the working fluid flowing through the channel at inlet temperature 300K. The Reynolds numbers are calculated based on (2.1). It is taken from different values of fluid velocity with reference to the hydraulic diameter.

3.2 Assumptions

Since the geometrical structure of the MCHS is congruent in each periodic section, only a single slice of microchannel was used in the simulation in order to optimize its computational time. The neighbouring solid surface and fluid flowing across it have been taken into account during the

simulation process. The following assumptions were also made in order to simplify the simulation model (Yadav et al., 2016) and at the same time, to ensure that sufficiently accurate result can be obtained:

- Plain water as working fluid,
- Steady flow, laminar, incompressible and Newtonian,
- Radiation heat transfer is neglected,
- Uniform heat flux throughout bottom wall.
- No-slip condition at wall.

Ansys Fluent 17.2 was employed, SIMPLE scheme was selected to solve the pressure-velocity coupling and the third order MUSCL (Monotonic Upstream Centered Scheme for conservation Laws) scheme was used for discretizing the convective term in the momentum and energy conservation equations. In order to obtain a converging solution, the residual criteria used for energy equation, continuity equation, and the velocity in the *x*, *y*, *z* direction are 1×10^{-7}, 1×10^{-4} and 1×10^{-6} respectively. A constant mesh size of 0.5μm and tetrahedron shape was used for all cases in the simulation. Since different heat sink materials were used, two different heat fluxes are applied at the bottom of the microchannel.

3.3 Validation of the Classical Model

Apart from the assumptions, several comparisons of our numerical simulation with experiment findings available in the literature were first performed to validate the proposed model. Figures 3.1 and 3.2 illustrate the

comparison of the numerical results with those obtained by Chai et al. (2013) and Steinke and Kandlikar (2005). A bare rectangular microchannel case was selected for comparison. As shown in the figures, the simulated data of Nusselt number versus Reynolds number and pressure drop versus Reynolds number in this study are in good agreement with the preceding findings. Therefore, the same scheme is applied to evaluate the performance of the MCHS developed using the extended surface heat transfer enhancement technique, the illustration of which shall be presented in the subsequent chapter.

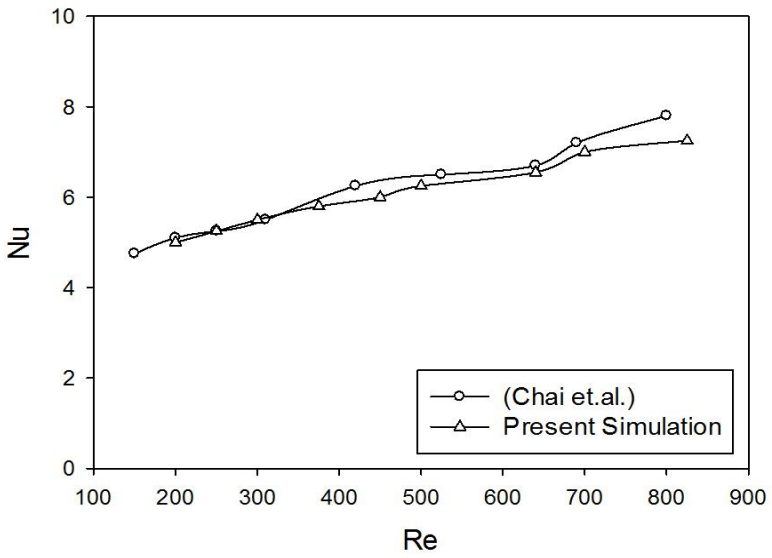

Figure 3.1: Comparison of Nusselt number versus Reynolds number

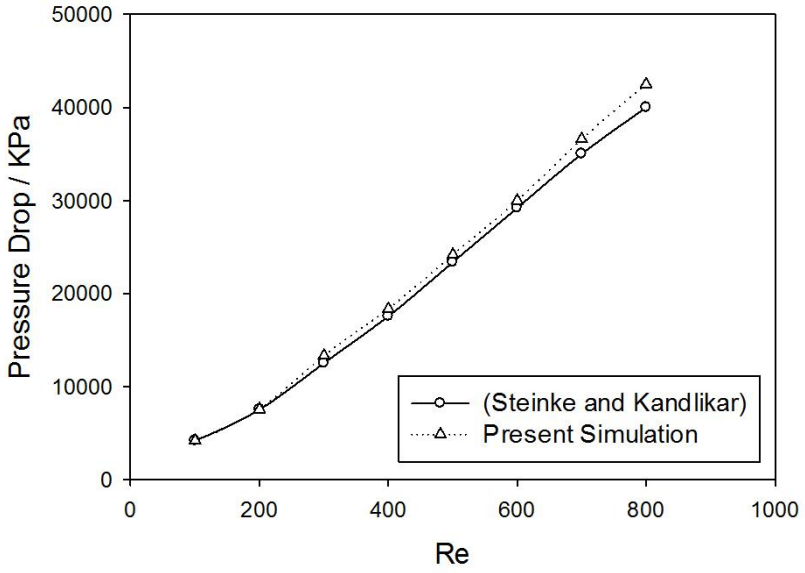

Figure 3.2: Comparison of Pressure drop versus Reynolds number

3.4 Experiment Model and Setup

Owing to the rapid development in the electronics industry, straight microchannel heat sinks could no longer meet the requirement of effective heat dissipation. As the fluid flows into the microchannel, the thickness of the thermal boundary layer increases. This phenomenon results in a steep temperature gradient between the core fluid and the fluid at the channel side wall, leading to inefficient heat transfer performance. Therefore, there is a need to look into some other techniques to enhance the performance of the heat sinks. Some of these techniques include manipulating the aspect ratio of the channel, varying the cross-section of the channel shape and increasing the surface roughness of the channel wall.

Studies demonstrated that the thermal boundary layer can be disrupted by introducing a flow disruption technique (Chai et al., 2013, Ghani et al., 2017, Wang et al., 2015). After reviewing the concept of these literature, a new design of micro-fins with diverging cylindrical geometry incorporated with different shapes of micro-ribs is proposed and simulated in this study. A combination of micro-fins with straight channel is presented in this chapter, the result of which would be subsequently discussed in following sub-section.

In the experiment, a microchannel with dimensions L = 50 mm, W = 3 mm, and H = 12 mm was fabricated. The diameter of the extended surface cylinder was set at 1 mm and the height of micro-fins was fixed to 5 mm. In order to prevent the redevelopment of the thermal boundary layer between the micro-fins, the fin-to-fin distance (pitch of fins) is set at 4.25 mm. The poly lactic acid (PLA) filament with aluminum metal mixture was selected as the heat sink material because it is relatively low in cost and can be easily fabricated using fused deposition modelling (FDM). Total of 12 channels were fabricated and a LED module with 35mm diameter was mount under the microchannel. The main aim of the experiment is to observe and verify the working principle of the microchannel heat sink and the effect of the micro-fins in the heat sink. The schematic diagrams of a bare microchannel heat sinks and a microchannel with micro-fins are shown respectively in Figures 3.3 and 3.4 while the dimensions of the microchannel is shown in Figure 3.5. The geometry parameter of Microchannel with micro-fins is illustrated in Table 3.1.

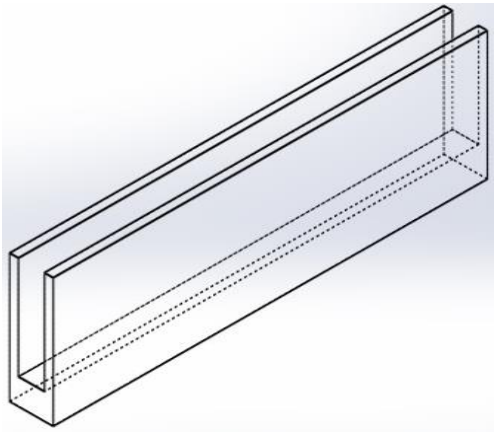

Figure 3.3:Schematic diagram of bare rectangular microchannel

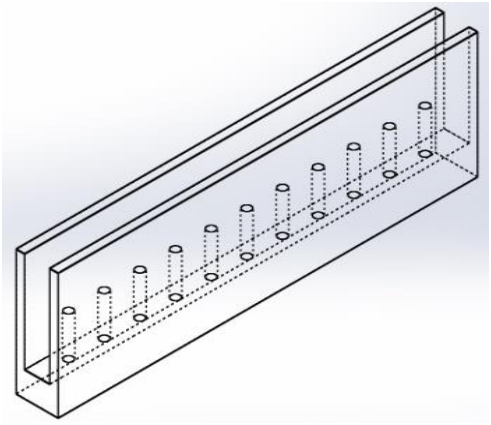

Figure 3.4: Schematic diagram of rectangular microchannel with micro-fins

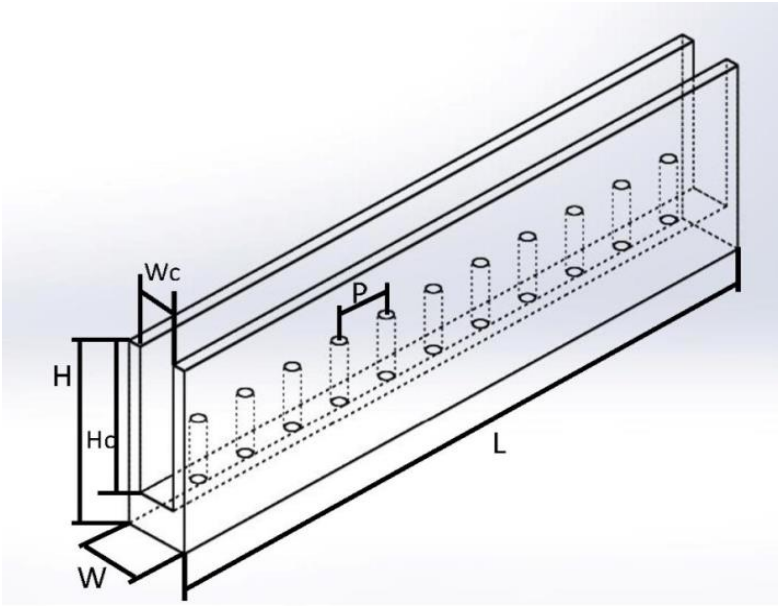

Figure 3.5: Dimension of Microchannel with micro-fins

Table 3.1: The geometry parameter of Microchannel with micro-fins

Parameter	Dimension (mm)
W	5.00
Wc	3.00
H	15.00
Hc	12.00
L	50.00
P	4.25

In the experiment, a total of 12 channels were fabricated to form the MCHS heat sink. As shown in Figures 3.6 and 3.7, the bare rectangular microchannel heat sink was fabricated using the fused deposition modelling (FDM) technique.

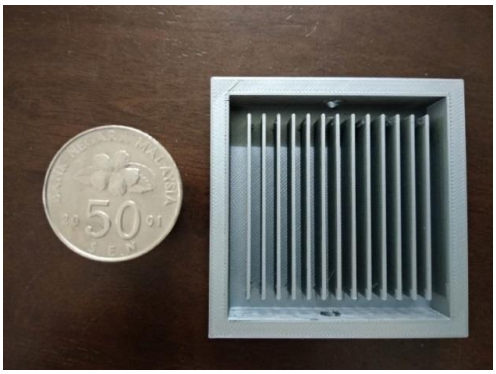

Figure 3.6: Fabricated bare rectangular microchannel heat sink

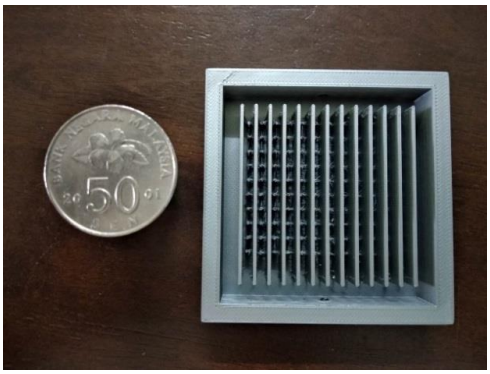

Figure 3.7: Fabricated rectangular microchannel heat sink with micro-fins

The experiment setup and the corresponding apparatus used in the setup are shown in Figures 3.8 and 3.9. The microchannel heat sink was then mounted with two connectors and transparent Perspex, as shown in Figure 3.10. The working fluid was initially fed from the water pump to the flow sensor. Constant fluid velocity $U = U_{in}$ and constant temperature T = 300 K were applied at the inlet of the MCHS. The flow rate was controlled by a flow meter. The fluid inlet and outlet were the narrowest part of the flow path and the diameter was 5 mm. The flow rate can be obtained based on the flow rate equation in (3.1) below:

$$Q_f = Au \tag{3.1}$$

where Q_f is the flow rate, A is the pipe area and u is the velocity of the fluid. When a flow rate of 4.6 ml/s is supplied into the microchannel heat sink, the fluid velocity is equal to 0.23 m/s. The Reynolds number corresponding to

0.23m/s is equivalent to 1200 and this value is known to be within the range of the laminar flow. Table 3.2 tabulates the variation of the flow rate and the velocity at different values of Reynolds number.

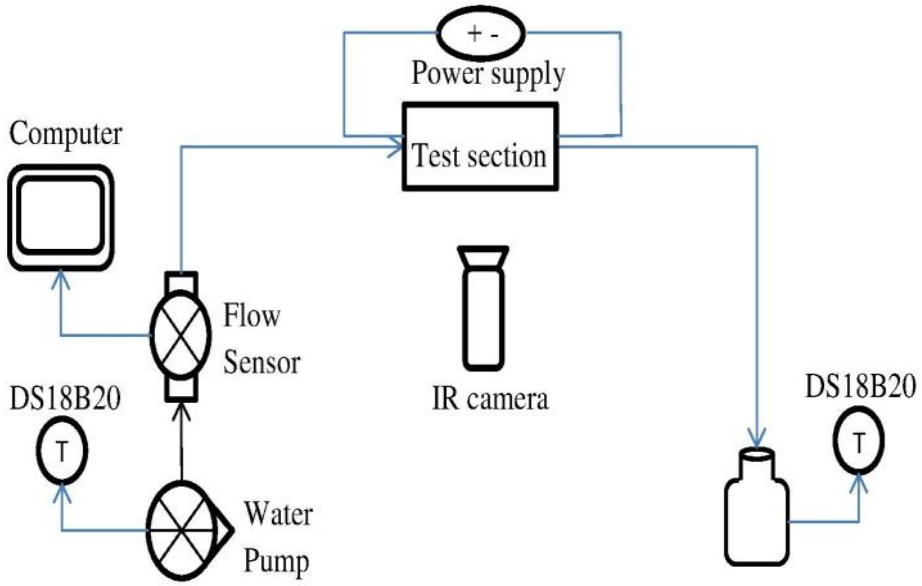

Figure 3.8: Schematic diagram of the experimental setup.

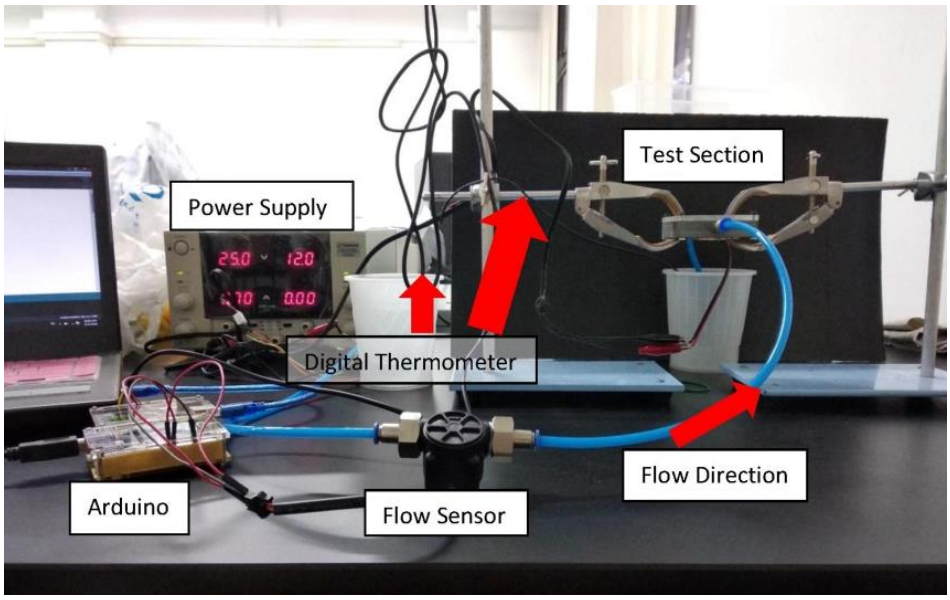

Figure 3.9: Image of the experimental setup.

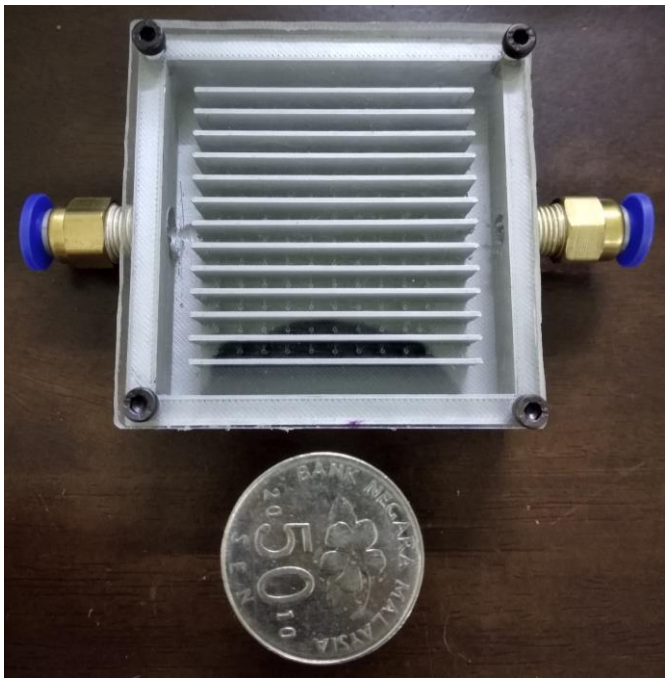

Figure 3.10: Image of microchannel heat sink after mounting

Table 3.2: The value of velocity and the flow rate at different Reynolds number

Reynolds number	Velocity (m/s)	Flow rate (ml/s)
400	0.078	1.53
600	0.107	2.3
800	0.156	3.06
1000	0.195	3.82
1200	0.234	4.60

The inlet and outlet fluid temperature were measured by using 2 digital thermometers (DS18B20 with an accuracy of ±0.5 °C) which were placed in the containers before and after the test section. At the test section in which the MCHS was placed, a heat source generated by an integrated LED light source (Cool RAY COB C46) was attached at the bottom of the MCHS heat sink. The LED light source provided approximately 10 W/cm^2 of heat flux. In the experiment, the top surface of the microchannel was covered by transparent

Perspex so as to provide an enclosed passage for fluid flow and to allow a better observation of the fluid flow. Four K type thermocouples with 1.5 mm probe diameter (PTMTCA7 with on accuracy of ±1.5 °C) and an IR camera (Fluke Tis55 Thermal Imager) were used to measure the temperature of the microchannel heat sink. The locations of the 4 thermocouples are 20 mm, 30 mm, 40 mm, and 50 mm respectively from the inlet and 1.5 mm above the bottom surface. Figure 3.11 shows the side view of the microchannel heat sink.

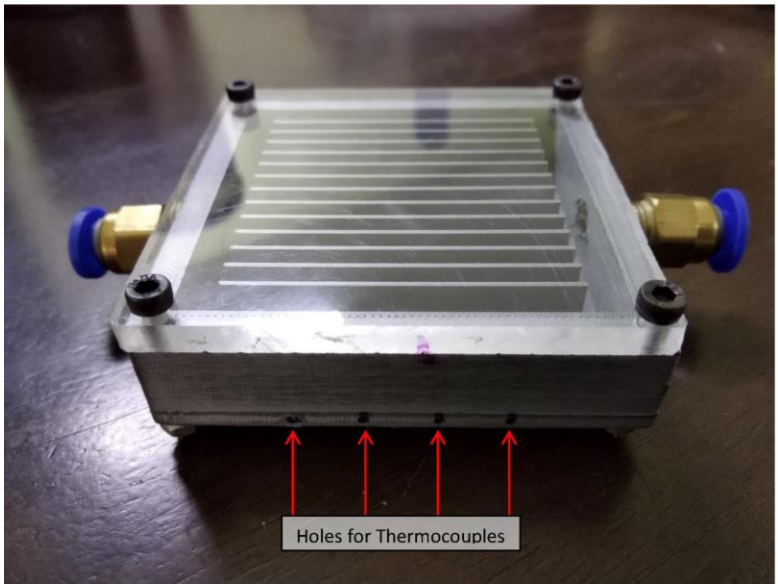

Figure 3.11: Image of the side view of microchannel heat sink after mounting

3.5 Experimental Results and Discussion

The experimental investigation was performed between $400 \leq Re \leq 1200$ and the heat flux through the bottom wall is 10 W/cm^2. The following results compared the temperature profile, velocity profile, pressure drop and thermal

performance of both microchannels. The effect of the micro-fins is discussed as well.

3.5.1 Velocity Distribution

Figures 3.12 and 3.13 show the fluid flow velocity of the bare rectangular microchannel and rectangular microchannel with micro-fins at Z-plane = 25 mm, Y-plane = 3.5 mm and Re = 1200. The fluid flow from the top to the bottom and the inlet velocity varies from 0.078 to 0.23 m/s.

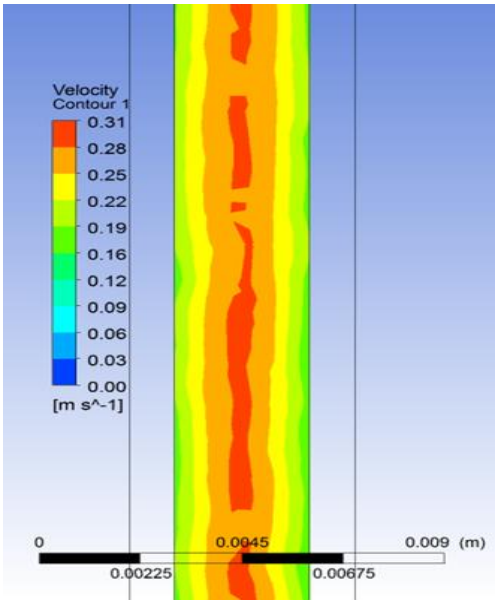

Figure 3.12: Velocity distribution of bare rectangular microchannel

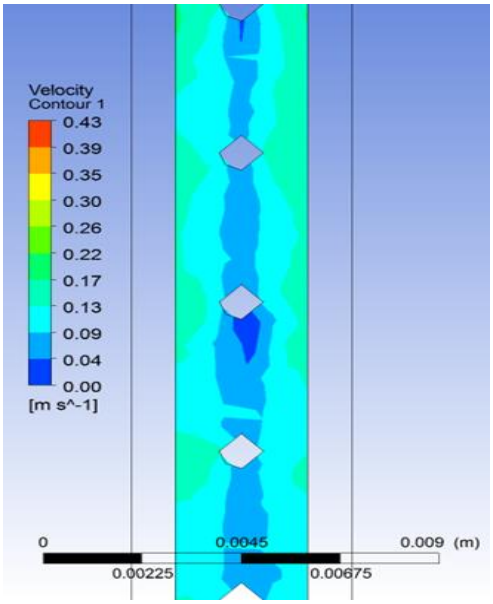

Figure 3.13: Velocity distribution of rectangular microchannel with micro-fins

From the simulation results, it can be observed that the fluid velocity of bare microchannel is higher compared to microchannel with micro-fins. The presence of micro-fins allocated at the middle of microchannel form obstacles to slow down the flow velocity. When the fluid flows through the micro-fins, core fluid at the middle impinges the micro-fins. A transverse flow is

produced concurrently due to the sudden contraction of the flow area at the micro-fins zone. As the core flow impinges the micro-fins, the core fluid is forced to move to the side wall, thus, the fluid velocity at the side wall increases slightly. When the fluid passes the micro-fins, the fluid velocity drastically decreases at the fin tail and a small area of stagnation zone is formed. When the fluid gushes into the microchannel heat sinks from a 5 mm diameter inlet, however, its velocity increases. As can be seen from both figures, the top fluid velocity increases, respectively, to 0.31 m/s and 0.43 m/s in the bare rectangular microchannel and the microchannel with micro-fins. Figures 3.14 and 3.15 show the simulated side view of the bare rectangular microchannel and rectangular microchannel with micro-fins.

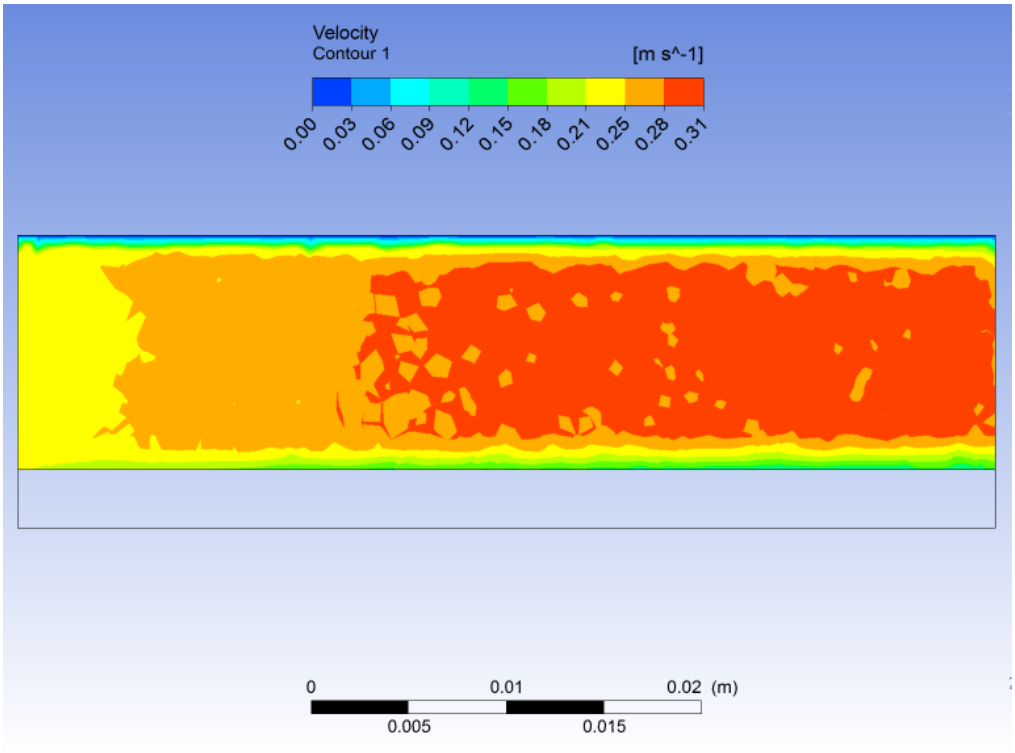

Figure 3.14: Velocity distribution of bare rectangular microchannel (side view)

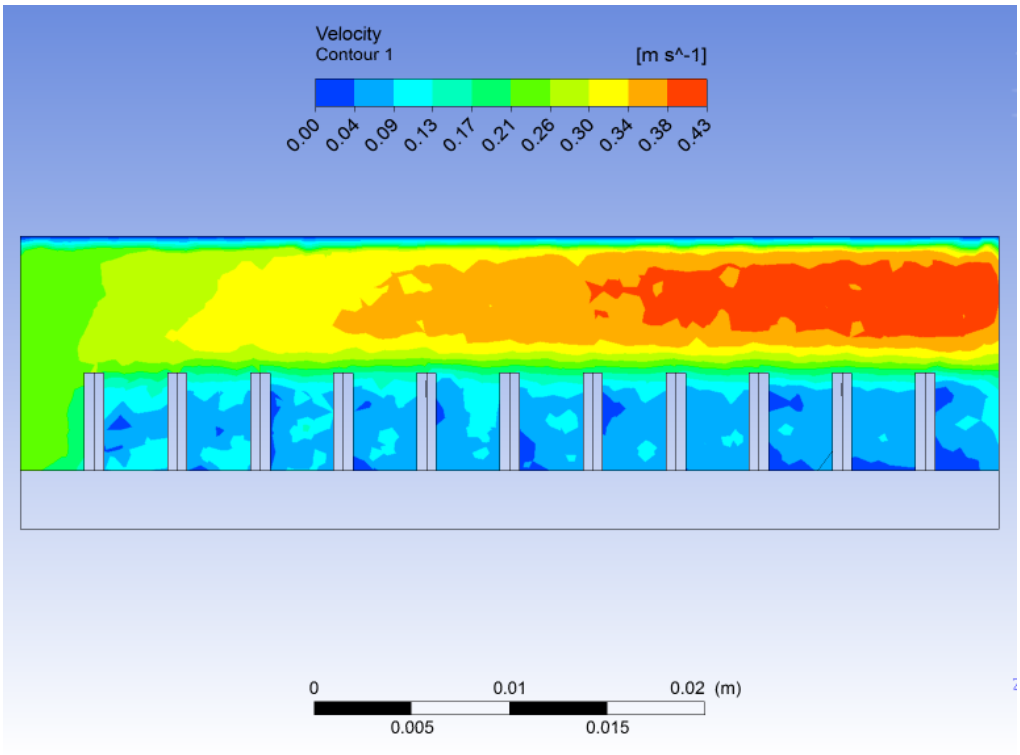

Figure 3.15: Velocity distribution of rectangular microchannel with micro-fins (side view)

Upon inspection on the side view of both microchannels, it can be seen that the high-velocity area of the microchannel with micro-fins was accumulated at the upper region as compared to the bare rectangular microchannel. This is because the presence of the micro-fins creates flow resistance at the bottom region of the microchannel where the heat flux is formed first.

3.5.2 Temperature Distribution

Figures 3.16 and 3.17 depict the simulated temperature distributions of the bare rectangular microchannel and the modified rectangular microchannel with micro-fins at Z-plane = 25 mm, Y-plane = 3.5 mm and Re = 1200. It is clear that the microchannel with micro-fins shows lower wall temperature

compared to the conventional bare microchannel. As shown from the top view of both microchannels, the fluid temperature at the middle of the bare microchannel is cooler compared to the microchannel with micro-fins. This phenomenon occurs when a fluid at a constant temperature flows over a surface that is at a different temperature. The layer of temperature difference between the fluid and the microchannel surface is known as the thermal boundary layer. In the bare rectangular microchannel, insufficient fluid mixing between the core flow and edge flow results in a continuous thickening of the thermal boundary layer and this leads to a poor heat transfer performance. The extended surface heat transfer enhancement technique introduces disturbance in the flow. The micro-fins which exist periodically at the middle of microchannel act as disrupters. They help to slow down the fluid velocity and induce recirculation flow to disrupt the thermal boundary layer. This result matches well with the studies conducted by Jia et al. (2018). Figures 3.18 and 3.19 show the side view of both microchannels.

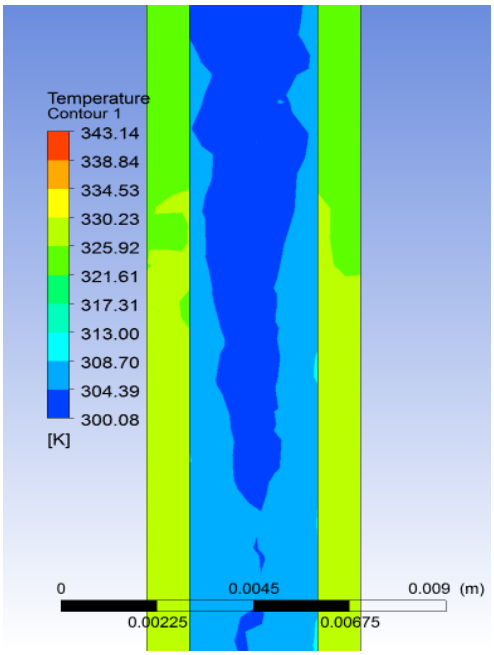

Figure 3.16: Temperature distribution of bare rectangular microchannel

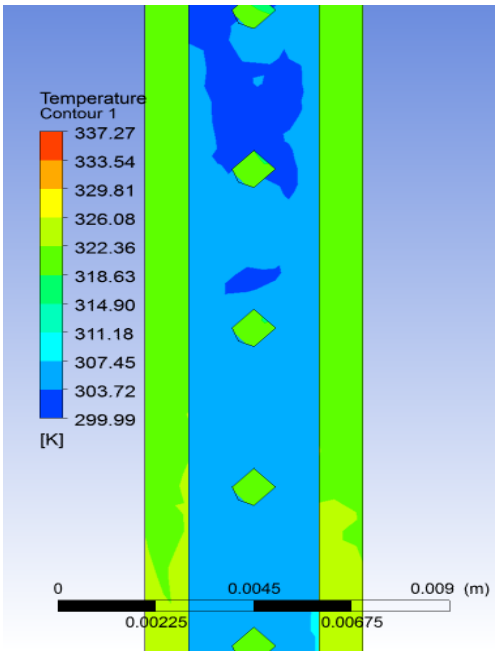

Figure 3.17: Temperature distribution of rectangular microchannel with micro-fins

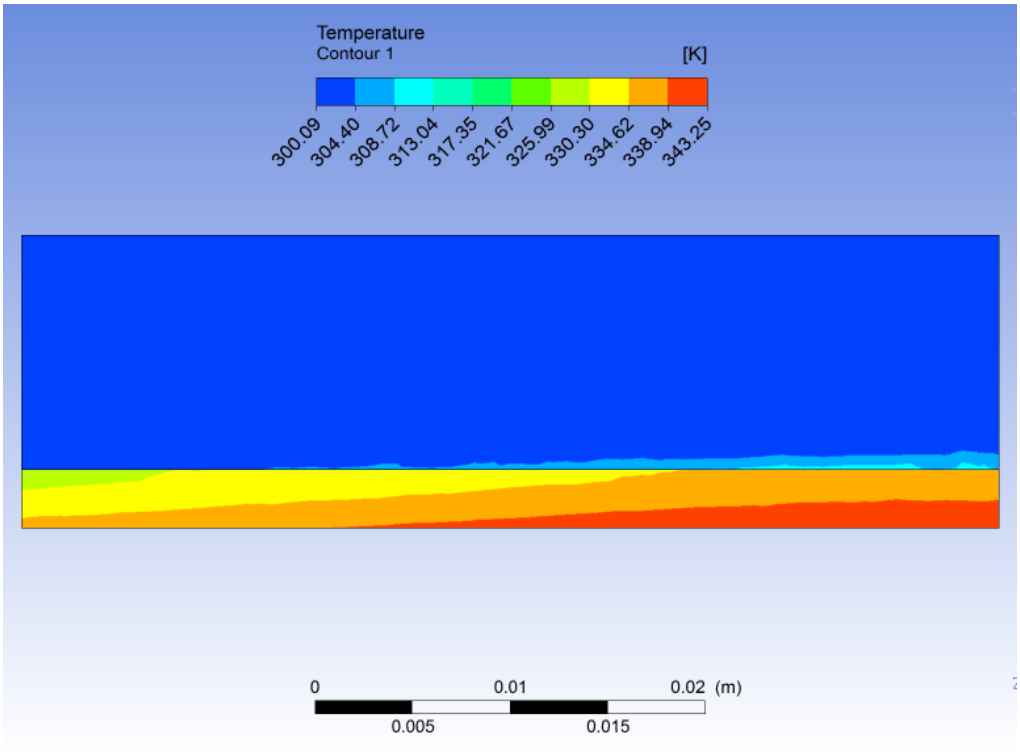

Figure 3.18: Temperature distribution of bare rectangular microchannel (side view)

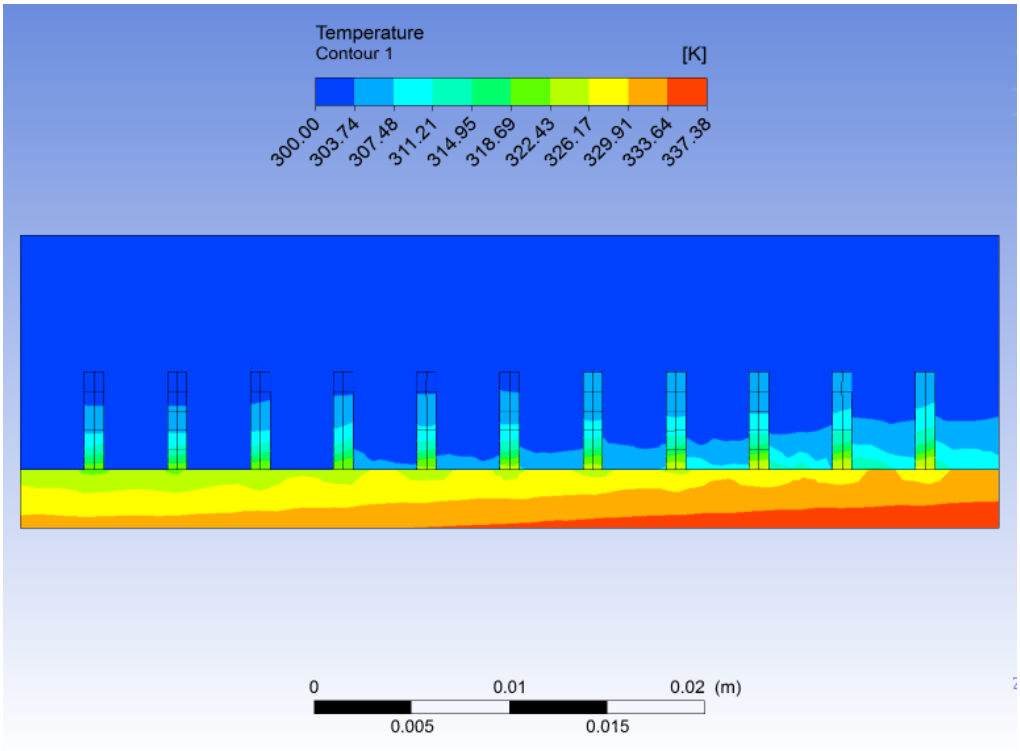

Figure 3.19: Temperature distribution of rectangular microchannel with micro-fins (side view)

The heat transfer characteristics of both microchannels also presented in terms of the Nusselt number as depicted in Figure 3.20. The experiment and simulation results of both microchannels show on increasing trend when the Reynolds number increases. It can be seen that the heat transfer of microchannel with micro-fins is enhanced as the Nusselt number of microchannel with micro-fins is higher compared to the conventional bare rectangular microchannel. This can be attributed to the presence of the micro-fins which produce a chaotic advection in the microchannel.

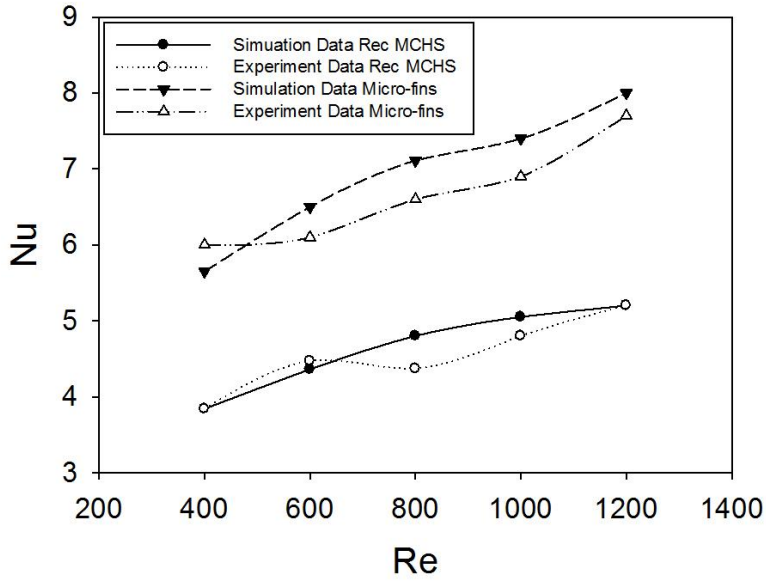

Figure 3.20: Variation of Nusselt number with Reynolds number

Four K-type thermocouples were used to measure the temperature of the microchannel heat sink (Detail reading is shown in appendix).The average readings of the four thermocouples were then compared to the simulation data. Tables 3.3 and 3.4 tabulate the experiment and simulation results of the wall temperature and Nusselt number. It is worthwhile noting that both the simulation and experiment results agree reasonably well. The maximum error of the conventional bare microchannel and the microchannel with micro-fins are 8.33%, 7.17% respectively. The reason for the error occurs is ascribed to the top cover of the microchannel heat sink. The top surface of the microchannel was assumed to be adiabatic in the simulation part for both cases. A clear Perspex cover was however used in the actual experiment. Hence, heat loss due to the Perspex cover exists in the experiment. A similar situation can be seen in Deng et al. (2015). Other than the top surface, the heat loss due to the outlet fluid may also contributes to the discrepancy. In the simulation, the

outlet temperature was taken at the end of the microchannel. Unlike the simulation, the outlet fluid temperature in the experiment was measured at the container which was connected to the microchannel with a 50 mm rubber tube.

Table 3.3: The experiment and simulation results of bare rectangular microchannel

Reynolds Number (RE)	**T_w (Simulation)**	**T_w (Experiment)**	**Nusselt Number (Simulation)**	**Nusselt Number (Experiment)**	**Discrepancy (%)**
400	353.0	347.1	3.84	3.83	0.26
600	348.0	343.7	4.36	4.47	2.52
800	346.0	341.8	4.80	4.40	8.33
1000	344.0	340.0	5.05	4.80	4.95
1200	343.0	339.0	5.20	5.19	0.19

Table 3.4: The experiment and simulation results of rectangular microchannel with micro-fins

Reynolds Number (RE)	**T_w (Simulation)**	**T_w (Experiment)**	**Nusselt Number (Simulation)**	**Nusselt Number (Experiment)**	**Discrepancy (%)**
400	347.0	340.0	5.65	6.00	6.20
600	342.0	337.0	6.50	6.10	6.15
800	340.0	335.0	7.11	6.60	7.17
1000	338.0	334.0	7.40	6.90	6,75
1200	337.0	333.7	8.00	7.70	3.75

3.5.3 Pressure drop and Overall Thermal Performance

Figure 3.21 shows the pressure drops of both microchannels with respect to the Reynolds number. As expected, the pressure drops of both microchannels increase when the Reynolds number increases. The result is similar with those reported in Zhang et al. (2010) and Jia et al. (2018). The pressure drops of the microchannel heat sink with micro-fins is higher compared to the bare rectangular microchannel heat sink. This is caused by the additional flow resistance introduced by the micro-fins. The micro-fins exist periodically at the middle of the microchannel. The fins therefore form a blocking effect to slow down the fluid velocity.

There is no doubt that the extended surface heat transfer enhancement technique could improve the heat transfer performance of a microchannel, but it is traded for the pressure drops. In this case, the overall thermal performance factor was calculated to supervise both heat transfer and pressure drop. Based on (2.5), the thermal performance factor of the microchannel heat sink with micro-fins is 1.168, 1.160, 1.123, 1.091, and 1.126 higher than the bare rectangular microchannel heat sink at 400, 600, 800, 1000 and 1200 Reynolds number respectively. It is clear that the thermal performance factor of the microchannel with micro-fins is greater than 1, which proves that this method could enhance the heat transfer performance in a microchannel.

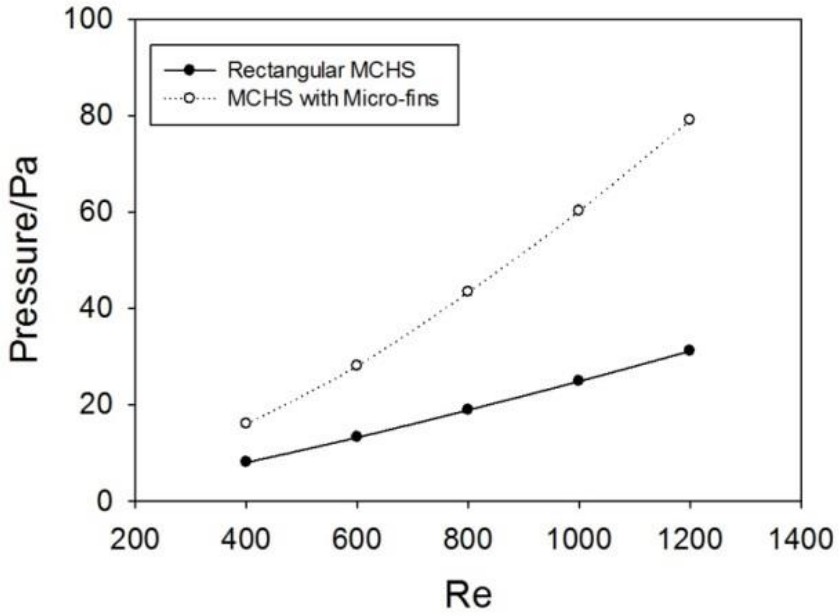

Figure 3.21: Variation of Pressure drop with Reynolds number of both microchannel heat sinks.

3.6 Concluding Remarks

In this chapter, the performance of microchannel heat sink with micro-fins is compared with the conventional bare microchannel heat sink. The overall thermal performance shows that the microchannel heat sink with micro-fins exhibits relatively better heat transfer characteristics.

CHAPTER 4

IMPROVEMENT IN MICROCHANNEL HEAT SINK WITH MICRO-FINS

4.1 Introduction

The experimental and simulation analyses performed in chapter 3 prove that the presence of micro-fins in a microchannel heat sink has significant influence in improving the heat transfer performance. This means that the micro-fins is capable of accelerating the temperature reduction pace. In this chapter, modifications on the geometry of the micro-fins are performed to further improve and enhance the heat transfer effectiveness in heat dissipation. The design were modified and simulated to validate their performance. The results obtained from the modified micro-fins are compared with the results of the conventional bare rectangular microchannel heat sink.

The overall dimensions of the microchannel are $36 \times 0.5 \times 0.7$ mm^3 ($L \times W \times H$); the fin height is 0.4 mm and the fin-to-fin distance (pitch of fins) is 3 mm. The aspect ratio (AR = H_{ch} / W_{ch}) and hydraulic diameter (d) are equal to 1.4 and 0.583 mm respectively. The dimension of the aspect ratio and hydraulic diameter was based on the numerical study of the heat transfer in a single microchannel Sahar et al. (2017). The author performed a series of simulations to investigate the effect of hydraulic diameter and aspect ratio on

the fluid flow and heat transfer. To achieve low pressure drop, the recommended aspect ratio lies between 1 and 2. The increase of hydraulic diameter results in an increase of the friction factor and average Nusselt number for simultaneously thermally and hydro-dynamically developing flow (Sahar et al., 2017).

4.2 Simulation Model I

When designing the microchannel heat sink (MCHS), several configurations of microchannel with micro-fins were simulated and analyzed under the same boundary condition and simulation environment as mentioned in section 3.2. A total of 6 different types of micro-fins were studied. In the simulation, the fluid velocity was set to be in the range of 0.689 to 2.07 m/s at 300K. A constant heat flux 100 W/cm^2 was applied at the bottom wall, aluminum alloy 6060 was selected as the material for the microchannel heat sink. For the sake of simplicity, the illustration of the simulations is divided into two sections.

In part I, three different configurations of microchannel heat sink with micro-fins; namely cylindrical micro-fins, offset cylindrical micro-fins, and diverging cylindrical micro-fin were introduced. Since the extended surface heat transfer enhancement technique produces the positive results, the geometry of the micro-fins was modified to introduce additional surface area of the fluid contact to the wall. Figures 4.1 to 4.4 show the configurations of

four different MCHSs and their corresponding dimensions are tabulated in Table 4.1.

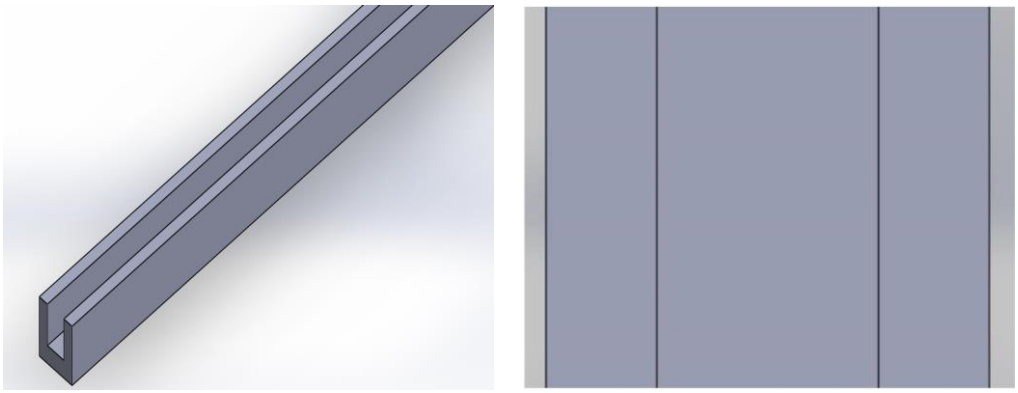

(a) (b)

Figure 4.1: The (a) overall and (b) top view of bare microchannel heat sink.

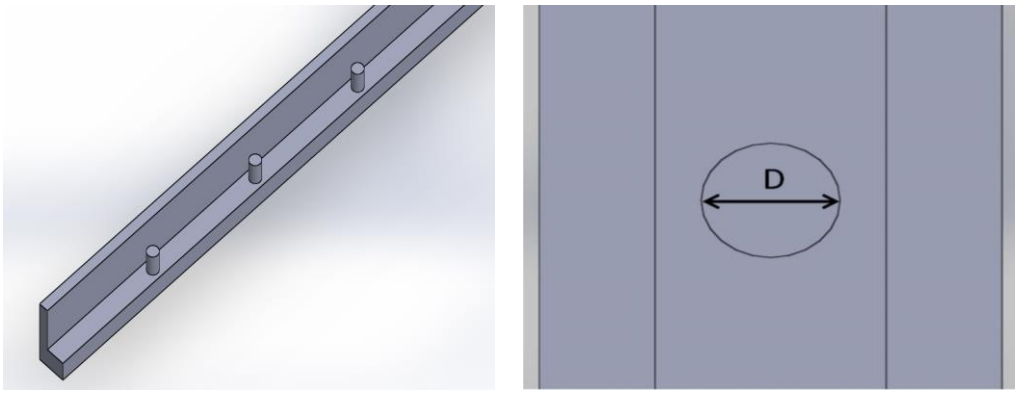

(a) (b)

Figure 4.2: The (a) overall and (b) top view of microchannel heat sink with cylindrical micro-fins.

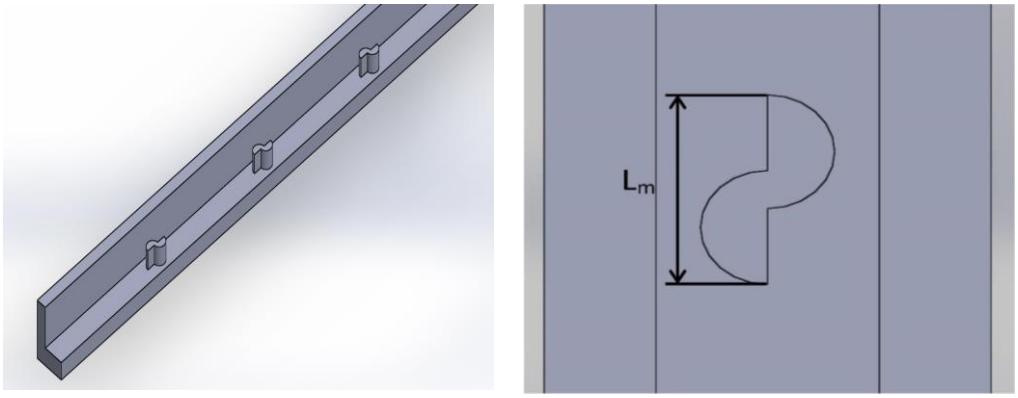

(a) (b)

Figure 4.3: The (a) overall and (b) top view of microchannel heat sink with offset cylindrical micro-fins.

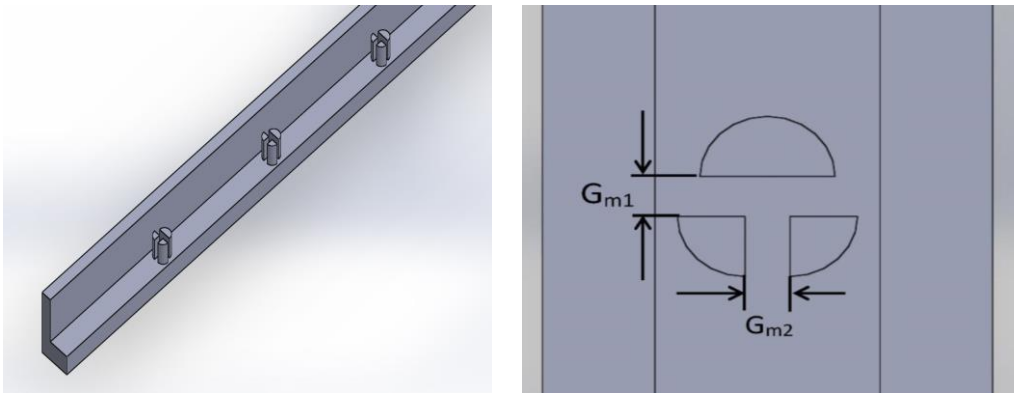

(a) (b)

Figure 4.4: The (a) overall and (b) top view of microchannel heat sink with diverging cylindrical micro-fins.

Table 4.1: The geometry parameter dimension of the micro-fins

Parameter	Dimension (mm)
D	0.30
L_m	0.50
G_{m1}	0.05
G_{m2}	0.05

4.2.1 Velocity Distribution

In this sub-section, the velocity contour is first discussed to evaluate the heat transfer performance of the proposed MCHS with micro-fins. Figures 4.5 to 4.7 show the velocity contour and velocity streamline of different geometries of micro-fins at Z-plane = 20 mm (i.e. the 6^{th} micro-fins from the inlet), Y-plane = 0.4 mm and Re = 600. The fluid was set to flow from the top to the bottom. From the results, it can be observed that the laminar stagnation zone is formed at the fin wake for all the three cases, with the diverging cylindrical micro-fin giving the worst result. This can be attributed to the

blocking effect which induces by the micro-fins. Although a similar effect was also found in the cylindrical micro-fins, the 90° turn in the flow path of the diverging micro-fins slows down the core flow significantly. Once the fluid impinges the micro-fins, the core flow is forced to move to both sides. This results in low flow velocity, which deteriorates further the laminar stagnation zone.

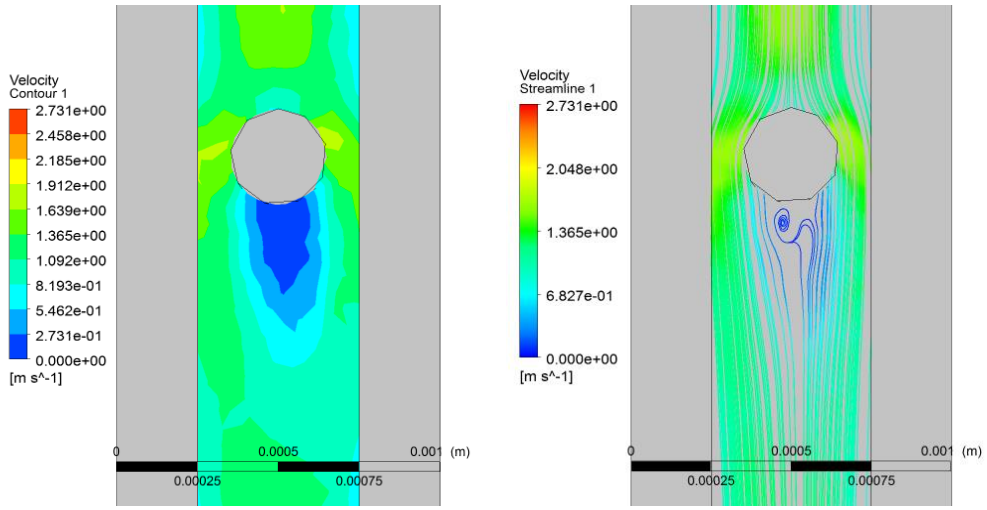

(a) (b)

Figure 4.5: The (a) velocity contour and (b) velocity streamline of microchannel heat sink with cylindrical micro-fins.

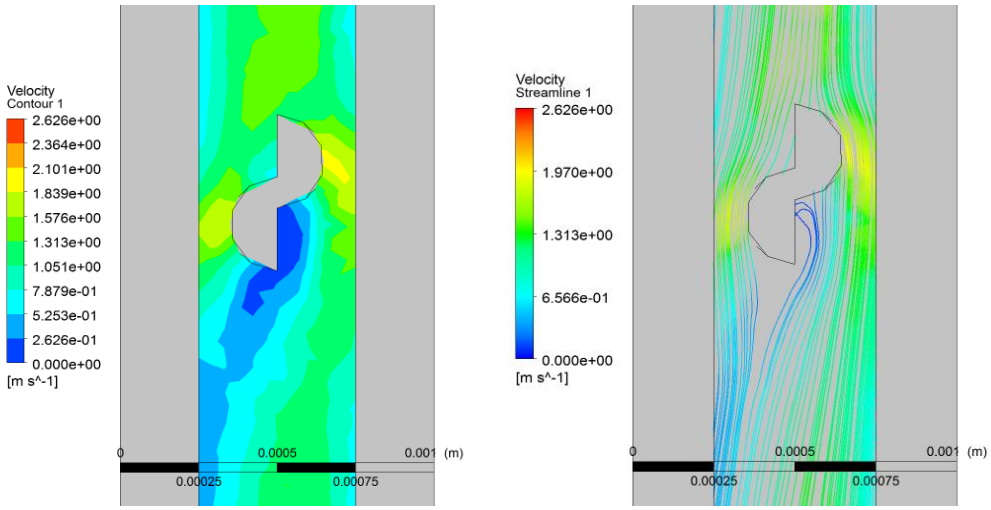

(a) (b)

Figure 4.6: The (a) velocity contour and (b) velocity streamline of microchannel heat sink with offset cylindrical micro-fins.

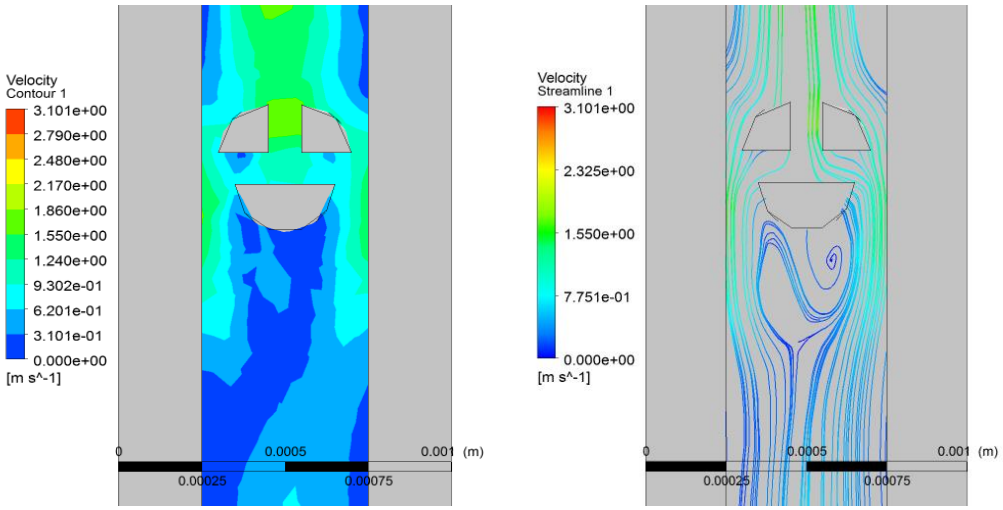

(a) (b)

Figure 4.7: The (a) velocity contour and (b) velocity streamline of microchannel heat sink with diverging cylindrical micro-fins.

4.2.2 Temperature Distribution

Figures 4.8 to 4.11 show the overall temperature distribution of the 4 types of MCHS. The average interface temperature of all the four types of MCHS is depicted in Figure 4.12. It is apparent that the average interface temperature of the microchannel heat sink decreases in all cases. The microchannels with micro-fin arrays (cylindrical micro-fins, offset cylindrical micro-fins and diverging cylindrical micro-fins) possess lower wall temperature as compared to the conventional bare rectangular microchannel. As discussed in section 3.5.2, this phenomenon is due to the chaotic advection introduced by the micro-fins. The high temperature regions in the microchannel with micro-fins have been reduced compared to those in the bare rectangular microchannel.

It is interesting to note that when the Reynolds number increases, the average interface temperature decreases proportionally. This can accredited to the increase of fluid velocity. When the Reynolds number increases, the fluid velocity increases as well. This is to say that there will be more fluid passing through the microchannel, resulting in better heat transfer performance. When the Reynolds number equal to 400, the average interface temperature of offset cylindrical micro-fins is lower compare to diverge cylindrical micro-fins, this can be explained based on Figures 4.6 and 4.7. At low flow rate, the fluid flow at the laminar stagnation zone formed after the diverging cylindrical micro-fins is so slow and approximate to zero flow rate. These trapped fluid deteriorated the heat transfer, but, this phenomena was resolve when the increasing of the Reynolds number.

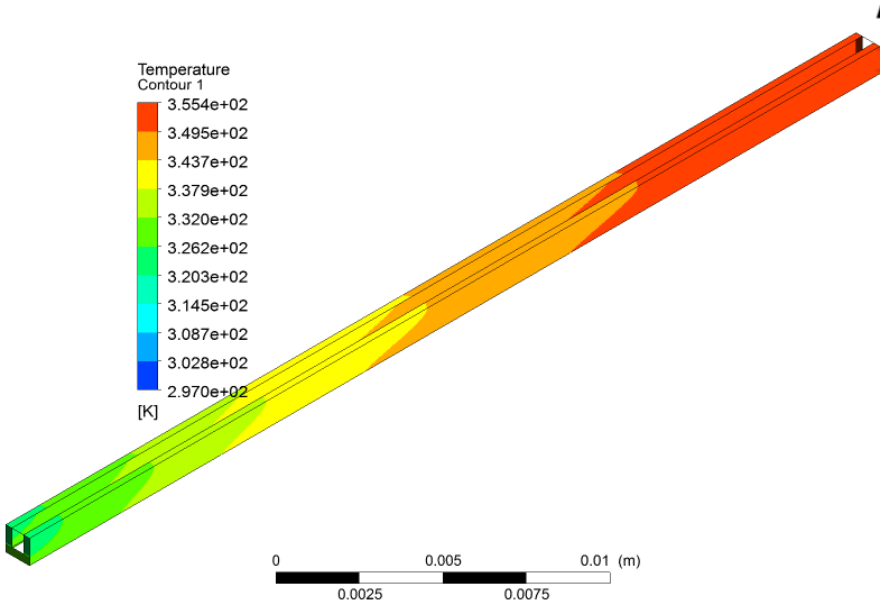

Figure 4.8: The temperature distribution of bare microchannel heat sink

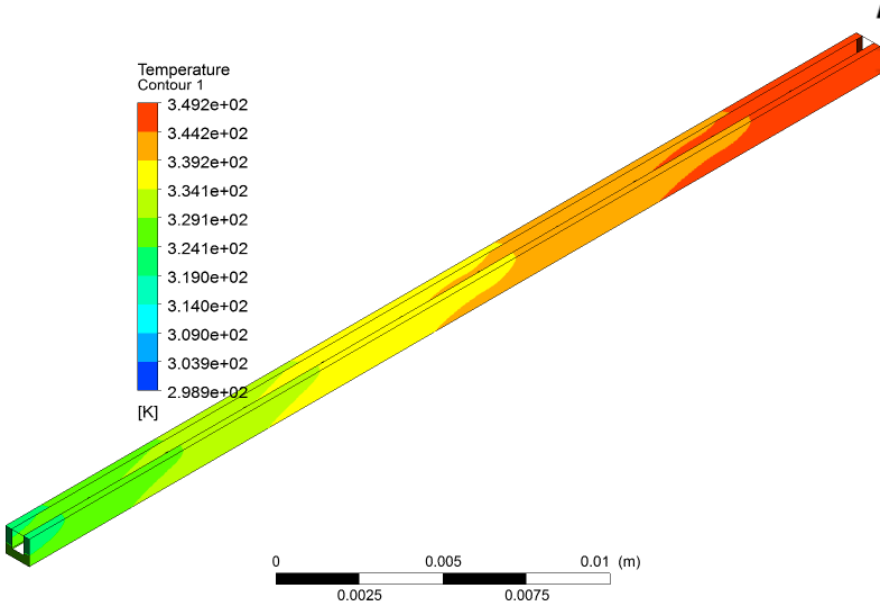

Figure 4.9: The temperature distribution of microchannel heat sink with cylindrical micro-fins.

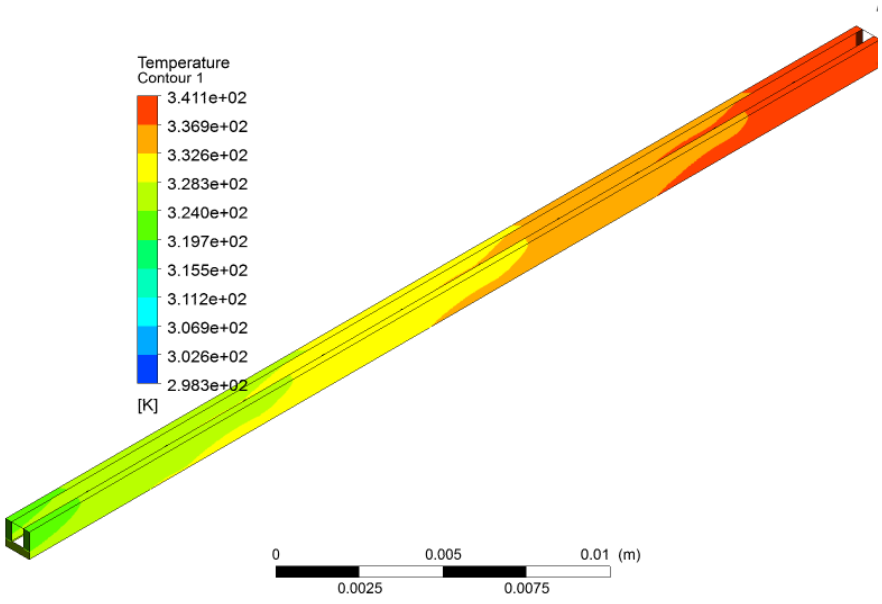

Figure 4.10: The temperature distribution of microchannel heat sink with offset cylindrical micro-fins.

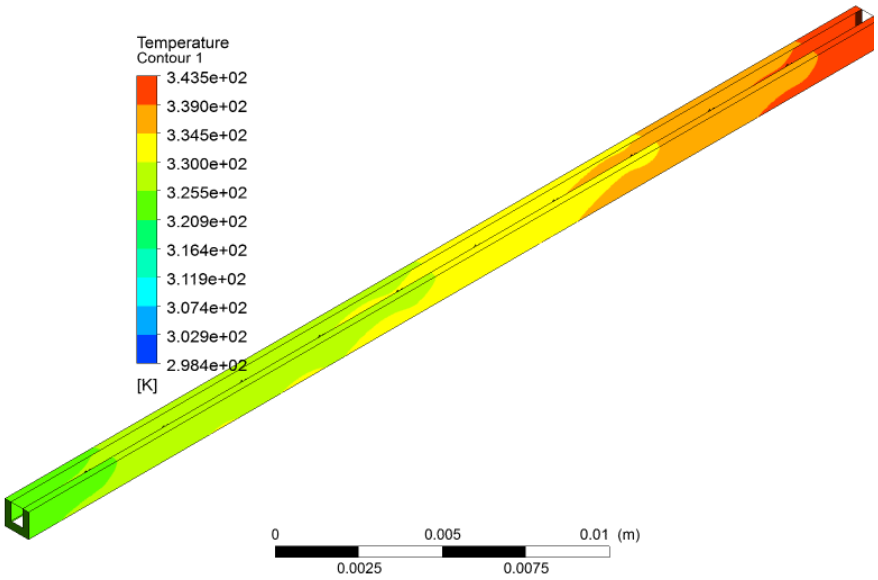

Figure 4.11: The temperature distribution of microchannel heat sink with diverging cylindrical micro-fins.

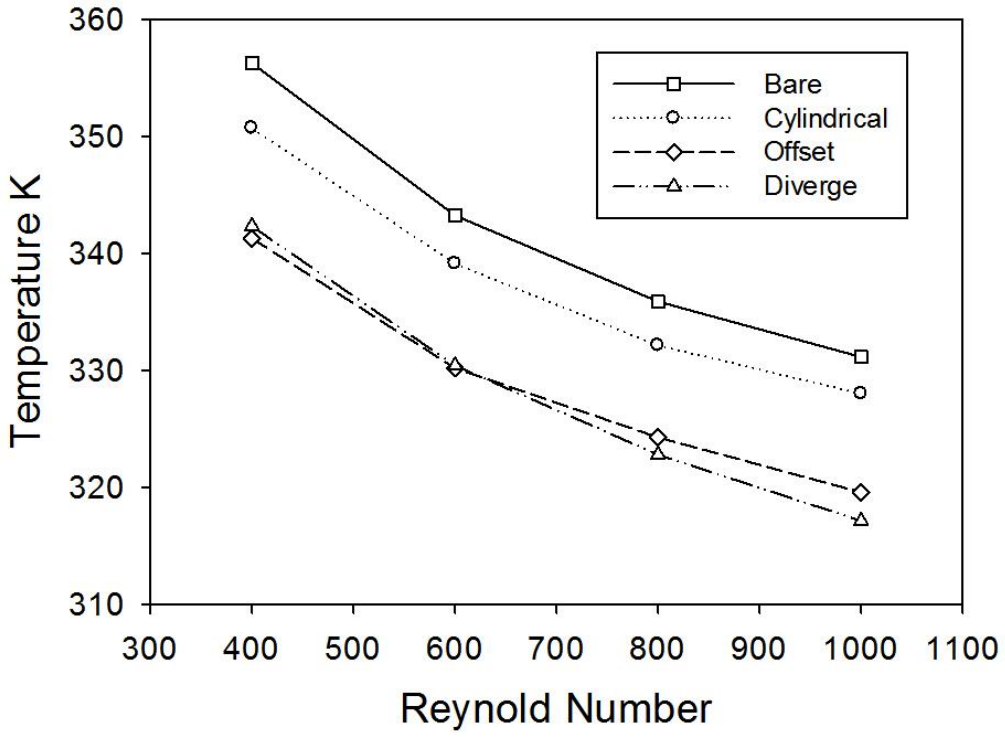

Figure 4.12: Graph of the average interface temperature.

4.2.3 Pressure drop characteristics

Figure 4.13 depicts the variation of pressure drop with Reynolds number. It is worthwhile noting that the pressure drop increases in all three cases as expected when compared to the bare rectangular microchannel. Among all the three cases, the diverging micro-fins has the highest pressure drop. This is due to the large area of stagnation zone formed at the end of the micro-fin. Since the micro-fins are located at the middle of the microchannel, the sudden contraction of flow area forces the core flow to squeeze to the side wall and a transverse flow is therefore produces. The velocity of the fluid decreases drastically at the micro-fins wake. Hence, the laminar stagnation zone is formed. This phenomenon is similar to the one reported in section 3.5.3, i.e. the diverging cylindrical micro-fins heat sink has higher pressure drop compared to its other counterparts. Considering the trade-off between heat dissipation performance and pressure drop, offset micro-fins design is considered as a more efficient design for better thermal management compared with the other microchannel heat sink.

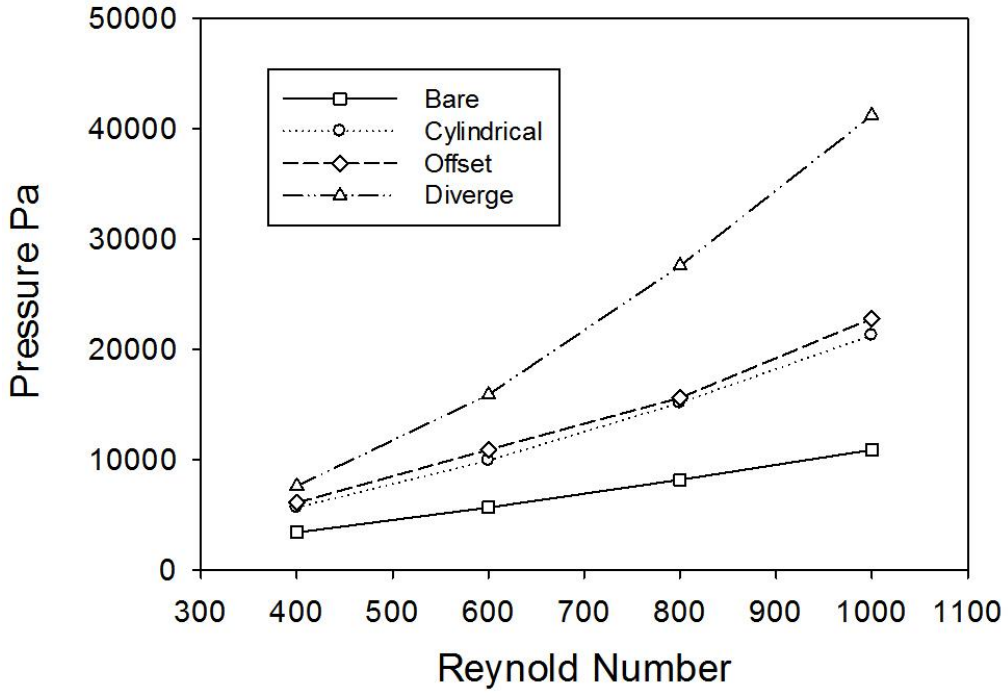

Figure 4.13: Variation of pressure drop with Reynolds number.

4.3 Simulation Model II

It is shown in the previous section that extended surface heat transfer enhancement technique imposes the penalty of pressure drop. Hence, modifications are performed on the micro-fins in heat sinks to minimize the impact of the pressure drop, while at the same time , to ensure the efficiency of its heat transfer characteristics. To do so, we combined the micro-fins together with the micro-ribs. Hence, four cases are investigated, namely the cylindrical micro-fins (Case A), diverging cylindrical micro-fins (Case B), diverging cylindrical micro-fins incorporated with semi-circle ribs (Case C), diverging cylindrical micro-fins incorporated with rectangular ribs (Case D) and diverging cylindrical micro-fins incorporated with triangular ribs (Case

E). The micro-ribs act as a disruptor and it is located at the center of the micro-fins. Figures 4.14 to 4.19 show the top view of the microchannel heat sink with different fin designs. The fluid was fed from the top to the bottom at 295 K. The overall dimensions of the microchannel are 36 × 0.5 × 0.7 mm^3, the height of the micro-fins is 0.4 mm and the fin-to-fin distance (pitch of fins) is 3 mm.

Figure 4.14: Configuration of Bare rectangular microchannel

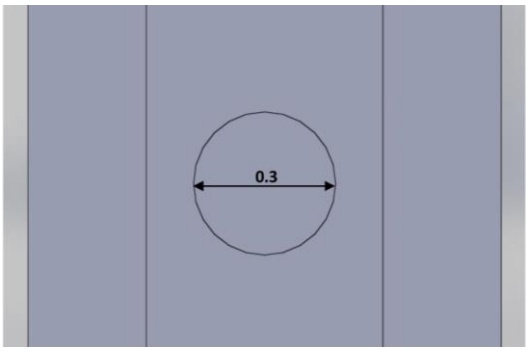

Figure 4.15: Configuration of case A

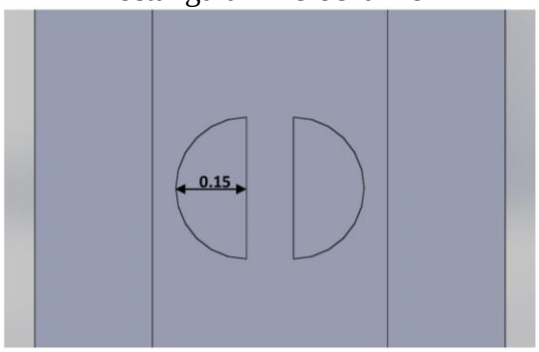

Figure 4.16: Configuration of Case B

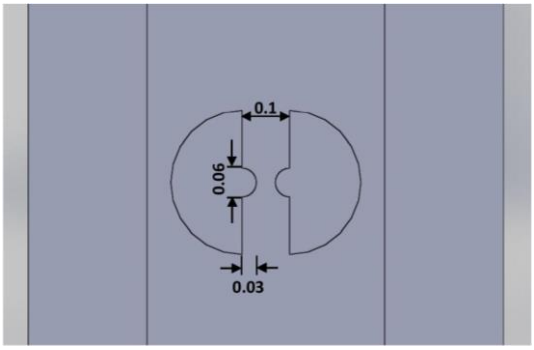

Figure 4.17: Configuration of case C

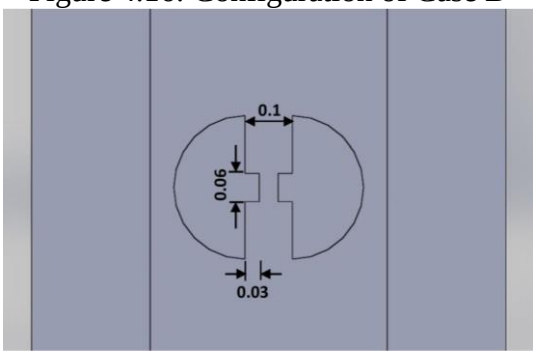

Figure 4.18: Configuration of Case D

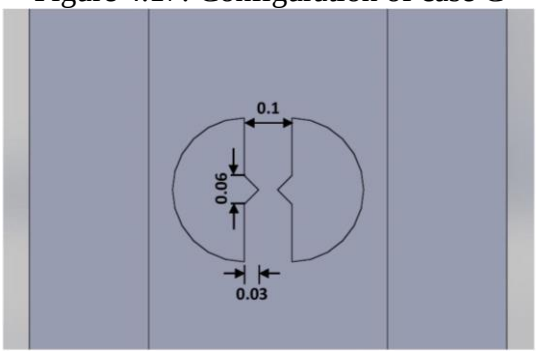

Figure 4.19: Configuration of case E

4.3.1 Velocity Distribution

Figures 4.20 to 4.25 illustrate the velocity distribution in the microchannel. As can be seen in Figure 4.20, the maximum velocity is located at the central portion of microchannel. The fast fluid flow at the middle portion mediates continuous thickening of thermal boundary layer. A significant temperature difference observed between the core flow and the edge flow leads to the poor heat transfer performance. As shown in Figures 4.21 and 4.22, the maximum velocity moves to both sides of the wall after the fluid impinges on the surface of the cylindrical micro-fins. Although the structure of the cylindrical micro-fins is able to interrupt the thermal boundary layer, it also creates a laminar stagnation zone after the micro-fins. The fluid flow rate is so slow at the laminar stagnation zone that the heat transfer rate declines as well.

The laminar stagnation in Figures 4.23 to 4.25 are relatively lower compared to Figure 4.21. We attribute this to the deviation of the micro-fins. The diverging part of the micro-fins allows the fluid to pass through while the micro-ribs disturb the flow on the high velocity region. The velocity gradient represents the hot and cold fluid mixing level. A lower velocity difference indicates a more superior level of the mixing. From the observation, Case C is formed to have better flow distribution than the other cases as the velocity gradient is smaller.

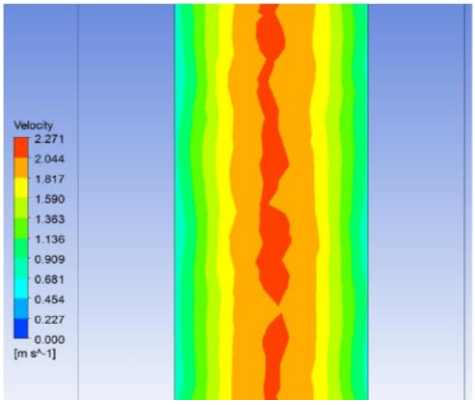

Figure 4.20: Velocity distribution of bare rectangular MCHS.

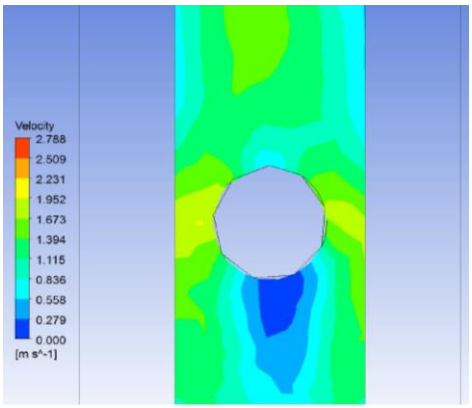

Figure 4.21: Velocity distribution of Case A.

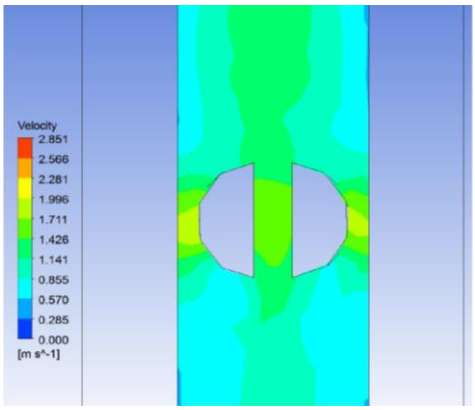

Figure 4.22: Velocity distribution of Case B.

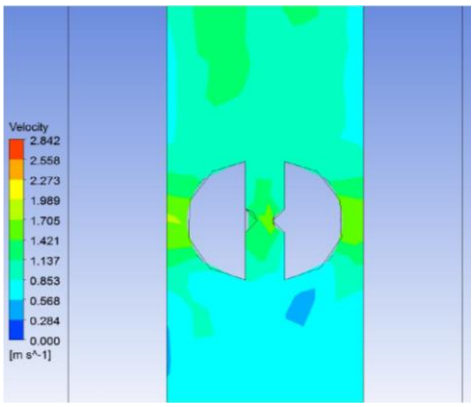

Figure 4.23: Velocity distribution of Case C.

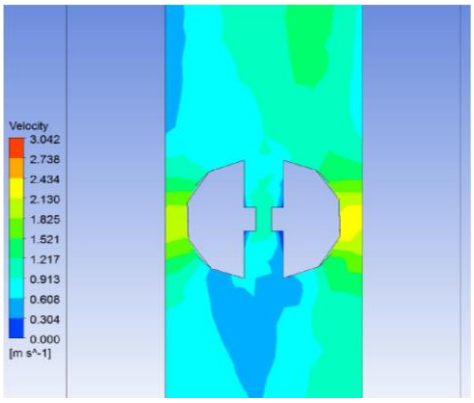

Figure 4.24: Velocity distribution of Case D.

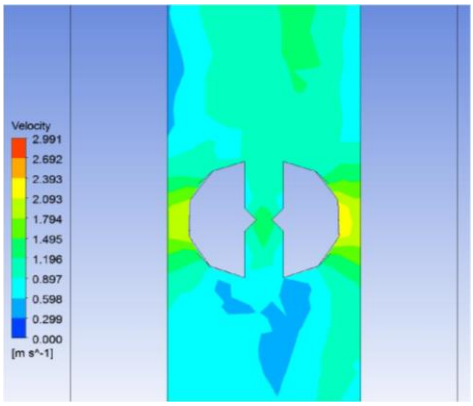

Figure 4.25: Velocity distribution of Case E.

4.3.2 Average Temperature and Heat Transfer Characteristics

Figure 4.26 depicts the relationship between the temperatures and the Reynolds number. It is obvious that the bare microchannel has the highest

temperature compared to the other designs. This phenomenon is caused by the continuous thickening of the thermal boundary layer along the straight microchannel. Besides, the average interface temperature of Case C is significantly reduced when compared to the bare rectangular microchannel. This can be accredited to the existence of micro-fins in the middle part of microchannel. The presence of the extended surface helps to disrupt the temperature profile and it prevents the thermal boundary layer to achieve a fully developed state. Meanwhile, the micro-fins redevelop the thermal boundary layer and thus augment the mixing of fluid at the side wall.

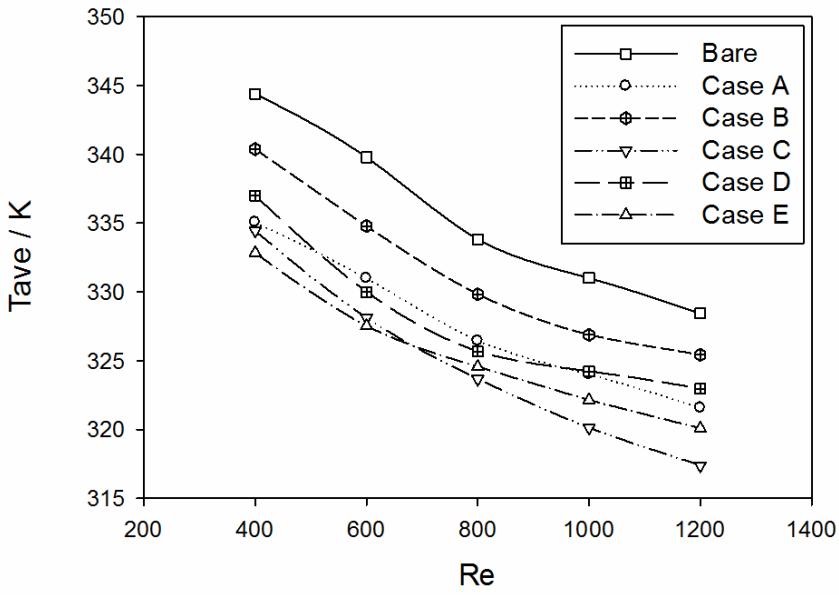

Figure 4.26: Average temperature versus Reynolds number at heat flux 100 W/cm^2.

1) Nusselt number is used to verify the heat characteristics of different configurations of microchannel heat sink. The overall Nusselt number is calculated from (2.3). Figure 4.27 plots the change of Nusselt number with different values of Reynolds number at heat flux of 100 W/m^2. As expected, the Nusselt number increases with the increasing Reynolds number in all

cases. In particular, the Nusselt number in all five non-bare designs is higher than that of the bare microchannel. The impact of Case C on the Nusselt number is similar to that caused in Case E, both of which are larger than those of Cases A, B and D. This could be attributed to the existence of semicircular and triangular ribs which shrink the laminar stagnation zone. A smaller laminar stagnation zone results in a more effective heat transfer in the microchannel. It is worthwhile noting that Case E exhibits relatively better performance at Reynolds number less than 700. This is because at Re < 700, the recirculation zone created by the triangular rib is smaller than rectangular rib, but slightly larger than the semicircular rib. Such phenomenon is reported in Wang at al., (2015). However, a decline in performance can be seen with further increase of the Reynolds number.

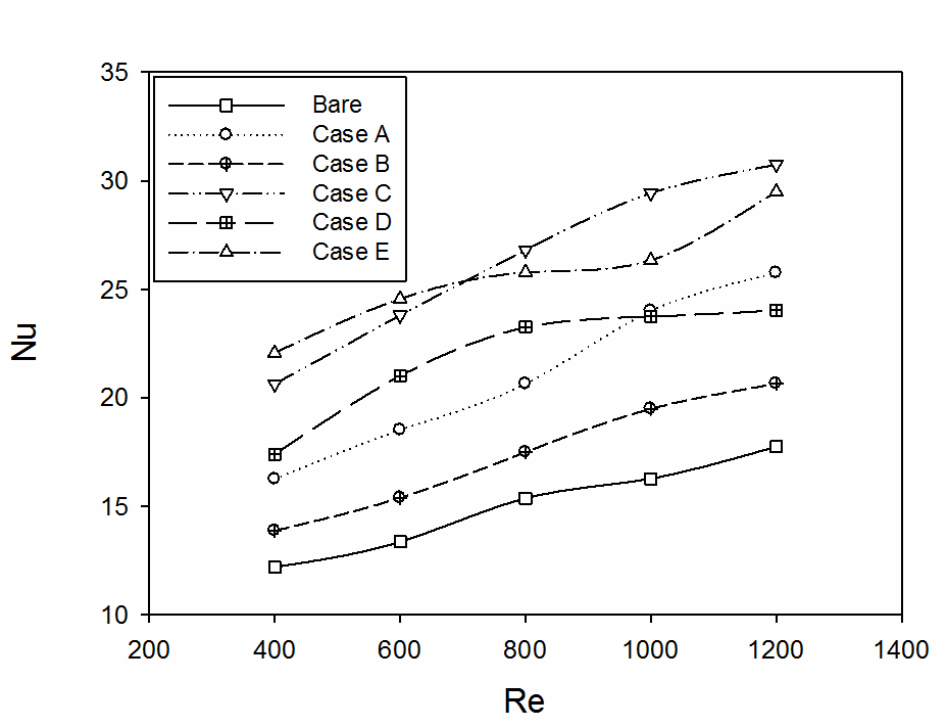

Figure 4.27: Variation of Nusselt number with Reynolds number

4.3.3 Pressure drop and overall thermal performance

Figure 4.28 depicts the pressure drop in all the microchannel heat sinks with respect to the Reynolds number. It can be seen that the pressure drop of the microchannels with micro-fins is higher compared to the bare microchannel. Apart from reducing their laminar stagnation zone, the pressure drops in Case C, D and E are also found to be higher than that in case A. We attribute this phenomenon to the increase of the cross-sectional area of the flow path. For instance, Case A and Case B have the same cross-sectional area of flow path, but the deviation of the micro-fins (Case B) allows the core fluid to flow continuously without be obstructed. Hence, the low pressure drops found is detected in Case B. For Case C, D and E, the micro-ribs are located at the centre of the micro-fins. The micro-fins act as a disruptor to slacken the fluid velocity, and this result in an increase of pressure drop.

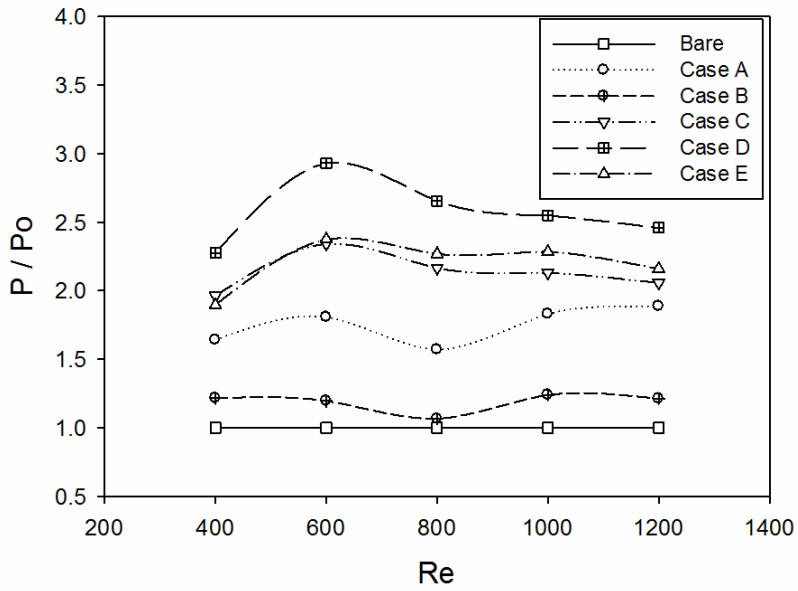

Figure 4.28: Pressure drop versus Reynolds number at heat flux 100 W/cm^2.

We have also evaluated the overall thermal performance of all the five cases and compared them with the bare rectangular microchannel. Figure 4.29 depicts the overall thermal performance of all the heat sink with respect to the Reynolds number. As can be clearly seen, the factor of the overall thermal performance for all the five cases was found to be greater than the conventional bare microchannel. This again proves that the extended surface in microchannel is important to improve the heat transfer performance of the microchannels. It is interesting to note that the thermal performance of case E is better than others before reaching the Reynolds number of 700. However, the performance of which deteriorates when the Reynolds number is greater than 700.

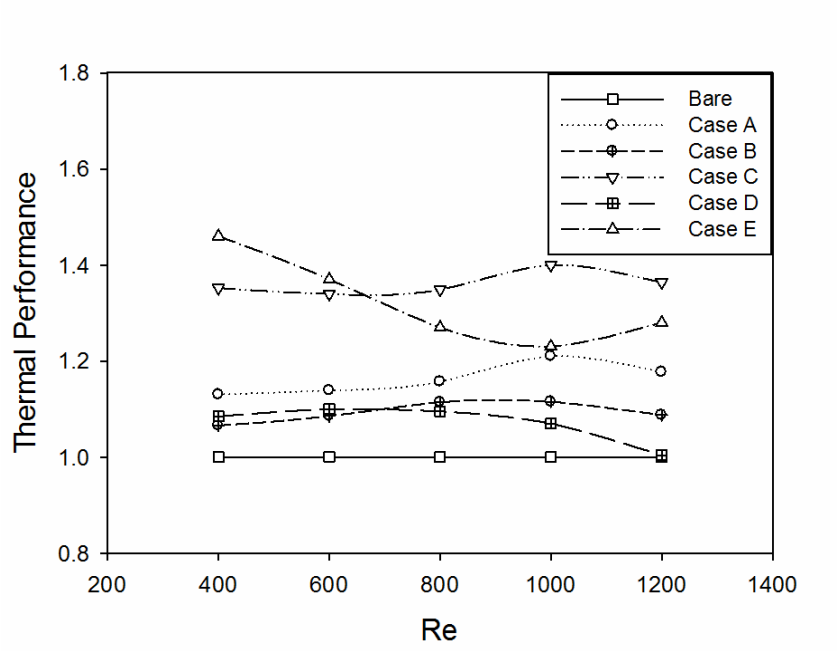

Figure 4.29: Variation of overall thermal performance with Reynolds number.

4.4 Concluding Remarks

In this chapter, 6 different types of microchannel with micro-fins were studied numerically. The performance of these microchannels with micro-fins is compared with the conventional bare microchannel heat sink. The results are evaluated based on the velocity distribution, heat transfer characteristics, pressure drop and the overall thermal performance. It is clearly seen that the extended surface heat transfer enhancement technique is again proved to have better thermal performance compared to the conventional bare rectangular microchannel. In particularly, the diverging cylindrical micro-fins incorporated with semi-circle micro-ribs (Case C) and diverging cylindrical micro-fins incorporated with triangular micro-ribs (Case E) have the highest overall thermal performance compared to other microchannel.

CHAPTER 5

CONCLUSION

Heat dissipation has become a major concern in electronic systems since the pass decades. Ever since Tuckerman and Pease (1981a) developed the first microchannel heat sink, it has become one of the most popular options to resolve heat dissipation issue in micro-scaled platforms. Due to its small hydraulic diameter, microchannel heat sinks provide high heat transfer coefficients and they do not have to rely much on coolant inventory. Since the heat fluxes have to be eliminated from the high power light emitting diodes (LEDs) and integrated circuits (ICs), the extended surface heat transfer enhancement techniques is selected to be implemented in the microchannel heat sinks. A microchannel heat sink MCHS with dimensions L = 50 mm, W = 3 mm, and H = 12 mm was fabricated and tested in this study. The collected results show that the heat transfer performance is augmented by the introduction of the extended surface cylinder in the microchannels. The MCHS with cylindrical micro-fins is able to reduce the average wall temperature to 333.7K when the Reynolds number equals 1200.

In order to further enhance the effectiveness of heat dissipation, modifications were performed on the extended surface micro-fins. A total of six different types of micro-fins were proposed in this study. For the sake of simplicity, the illustration of the simulations is divided into two sections. In section I, the geometry of the micro-fins was modified to introduce additional

surface area of the fluid contact to the wall. However, in the section II, the improvements of the micro-fins were based on the shortcoming of the section I. In section I, the diverging cylindrical micro-fins heat sink is found to exhibit the lowest average wall temperature when the Reynolds number is equal to 1000. The pressure drop of the heat sink, however, is directly proportional to the Reynolds number. Even so, the pressure drop in the heat sink is within an acceptable level. Hence, the offset cylindrical micro-fins heat sink is considered to be an excellent candidate to be used for heat dissipation.

Since the designs in Section I result in an increase in pressure drop, modifications were performed on the micro-fins to minimize the impact of the pressure drop. The modifications on the micro-fins were rather laborious since the efficiency of the heat transfer characteristics has to be taken into consideration. This is to say that, the geometry of the microchannel heat sinks has to be adjusted to minimize the pressure drop within the devices; while at the same time, the effectiveness of heat dissipation is to be maintained as well. A comparative study of 4 different types of micro-fins was conducted in section II. Based on the findings, the diverging cylindrical micro-fins incorporated with micro-ribs shows the lowest velocity difference which indicates a more superior level of the fluid mixing and this result in a better heat transfer performance. As compared to the diverging cylindrical micro-fins in section I (i.e 4 times higher than the conventional bare rectangular microchannel heat sink), the pressure drop of the diverging cylindrical micro-fins incorporated with micro-ribs (Case C and Case E) have successfully reduced by twice that of the bare rectangular microchannel heat sink. In

particular, the diverging cylindrical micro-fins incorporated with triangular ribs (Case E) can be employed at low Reynolds number. But when the Reynolds number increases, the overall thermal performance of the diverging cylindrical micro-fins incorporated with semi-circle ribs (Case C) is relatively better. This is due to the fact that the diverging micro-fins heat sink with semi-circle ribs (i.e. Case C) mediates the redevelopment of thermal boundary layer, which in turn, enhances the heat transfer rate. The overall thermal performance of Case C is found to be 1.4 times greater than that of the bare microchannel heat sink.

Clearly, the extended surface heat transfer enhancement technique produces positive results in the single phase microchannel heat sinks. Hence, the following studies could be performed for future improvements in heat sinks:

(i) Extended surface heat transfer enhancement technique could be applied in the two phase flow microchannel heat sinks so as to obtain a more effective and efficient cooling device for heat dissipation.

(ii) Replace the working fluid with various types of nano-fluid and observe the impact of these nano-fluids on the heat transfer performance.

REFERENCE

ABUBAKAR, S. & SIDIK, N. C. 2015. Numerical prediction of laminar nanofluid flow in rectangular microchannel heat sink. *J. Adv. Res. Fluid Mech. Therm. Sci.,* 7**,** 29-38.

AGOSTINI, B., FABBRI, M., PARK, J. E., WOJTAN, L., THOME, J. R. & MICHEL, B. 2007. State of the art of high heat flux cooling technologies. *Heat Transfer Engineering,* 28**,** 258-281.

ANDERSON, J. 1992. Governing equations of fluid dynamics. *Computational fluid dynamics.* Springer.

BAVIÈRE, R., FAVRE-MARINET, M. & LE PERSON, S. 2006. Bias effects on heat transfer measurements in microchannel flows. *International Journal of Heat and Mass Transfer,* 49**,** 3325-3337.

BERGLES, A. & DORMER JR, T. 1969. Subcooled boiling pressure drop with water at low pressure. *International Journal of Heat and Mass Transfer,* 12**,** 459-470.

BOWERS, M. & MUDAWAR, I. 1994a. High flux boiling in low flow rate, low pressure drop mini-channel and micro-channel heat sinks. *International Journal of Heat and Mass Transfer,* 37**,** 321-332.

BOWERS, M. B. & MUDAWAR, I. 1994b. Two-phase electronic cooling using mini-channel and micro-channel heat sinks: part 1—design criteria and heat diffusion constraints. *Journal of Electronic Packaging,* 116**,** 290-297.

BOWERS, M. B. & MUDAWAR, I. 1994c. Two-Phase Electronic Cooling Using Mini-Channel and Micro-Channel Heat Sinks: Part 2—Flow Rate and Pressure Drop Constraints. *Journal of Electronic Packaging,* 116**,** 298-305.

BOX, M. 1965. A new method of constrained optimization and a comparison with other methods. *The Computer Journal,* 8**,** 42-52.

CHAI, L., XIA, G., WANG, L., ZHOU, M. & CUI, Z. 2013. Heat transfer enhancement in microchannel heat sinks with periodic expansion–constriction cross-sections. *International Journal of Heat and Mass Transfer,* 62**,** 741-751.

CHAI, L., XIA, G. D. & WANG, H. S. 2016. Numerical study of laminar flow and heat transfer in microchannel heat sink with offset ribs on sidewalls. *Applied Thermal Engineering,* 92**,** 32-41.

CHOI, S. 1991. Fluid flow and heat transfer in microtubes. *Micromechanical Sensors, Actuators, and Systems, ASME*, 123-134.

CHONG, S., OOI, K. & WONG, T. 2002. Optimisation of single and double layer counter flow microchannel heat sinks. *Applied Thermal Engineering,* 22**,** 1569-1585.

DENG, D., WAN, W., TANG, Y., SHAO, H. & HUANG, Y. 2015. Experimental and numerical study of thermal enhancement in reentrant copper microchannels. *International Journal of Heat and Mass Transfer*, 91**,** 656-670.

DO NASCIMENTO, F. J., LEÃO, H. L. S. L. & RIBATSKI, G. 2013. An experimental study on flow boiling heat transfer of R134a in a microchannel-based heat sink. *Experimental Thermal and Fluid Science,* 45**,** 117-127.

GHALE, Z. Y., HAGHSHENASFARD, M. & ESFAHANY, M. N. 2015. Investigation of nanofluids heat transfer in a ribbed microchannel heat sink using single-phase and multiphase CFD models. *International Communications in Heat and Mass Transfer*, 68**,** 122-129.

GHANI, I. A., KAMARUZAMAN, N. & SIDIK, N. A. C. 2017. Heat transfer augmentation in a microchannel heat sink with sinusoidal cavities and rectangular ribs. *International Journal of Heat and Mass Transfer,* 108**,** 1969-1981.

GUI, F. & SCARINGE, R. P. 1995. Enhanced heat transfer in the entrance region of microchannels. American Society of Mechanical Engineers, New York, NY (United States).

GUNNASEGARAN, P., SHUAIB, N., MOHAMMED, H., JALAL, M. A. & SANDHITA, E. 2012. Heat transfer enhancement in microchannel heat sink using nanofluids. *Fluid Dynamics, Computational Modeling and Applications.* InTech.

GUO, Z.-Y. & LI, Z.-X. 2003. Size effect on microscale single-phase flow and heat transfer. *International Journal of Heat and Mass Transfer,* 46**,** 149-159.

HARMS, T. M., KAZMIERCZAK, M. J. & GERNER, F. M. 1999. Developing convective heat transfer in deep rectangular microchannels. *International Journal of Heat and Fluid Flow*, 20**,** 149-157.

HATAMI, M. & GANJI, D. 2014. Thermal and flow analysis of microchannel heat sink (MCHS) cooled by Cu–water nanofluid using porous media approach and least square method. *Energy Conversion and management,* 78**,** 347-358.

HEGDE, P. G. 2006. *MICROCHANNEL HEAT SINKS FOR COOLING HIGH HEAT FLUX ELECTRONIC DEVICES—ANALYSIS WITH SINGLE AND TWO PHASE FLOWS*. Ph. D. Thesis, University of Science, Malaysia.

HONG, F. & CHENG, P. 2009. Three dimensional numerical analyses and optimization of offset strip-fin microchannel heat sinks. *International Communications in Heat and Mass Transfer,* 36**,** 651-656.

HUSAIN, A. & KIM, K.-Y. 2008. Microchannel heat sink with designed roughness: analysis and optimization. *Journal of Thermophysics and Heat Transfer,* 22**,** 342-351.

JIA, Y., XIA, G., LI, Y., MA, D. & CAI, B. 2018. Heat transfer and fluid flow characteristics of combined microchannel with cone-shaped micro pin fins. *International Communications in Heat and Mass Transfer,* 92**,** 78-89.

JUDY, J., MAYNES, D. & WEBB, B. 2002. Characterization of frictional pressure drop for liquid flows through microchannels. *International Journal of heat and mass transfer,* 45**,** 3477-3489.

KALTEH, M., ABBASSI, A., SAFFAR-AVVAL, M., FRIJNS, A., DARHUBER, A. & HARTING, J. 2012. Experimental and numerical investigation of nanofluid forced convection inside a wide microchannel heat sink. *Applied Thermal Engineering,* 36**,** 260-268.

KANDLIKAR, S. & BALASUBRAMANIAN, P. Extending the applicability of the flow boiling correlation to low Reynolds number flows in microchannels. ASME 2003 1st international conference on microchannels and minichannels, 2003. American Society of Mechanical Engineers, 603-608.

KANDLIKAR, S. G. 1990. A general correlation for saturated two-phase flow boiling heat transfer inside horizontal and vertical tubes. *Journal of heat transfer,* 112**,** 219-228.

KANDLIKAR, S. G. & BALASUBRAMANIAN, P. 2004. An extension of the flow boiling correlation to transition, laminar, and deep laminar flows in minichannels and microchannels. *Heat Transfer Engineering,* 25**,** 86-93.

KANDLIKAR, S. G. & STEINKE, M. E. 2002. Contact angles and interface behavior during rapid evaporation of liquid on a heated surface. *International Journal of Heat and Mass Transfer,* 45**,** 3771-3780.

KAWAHARA, A., CHUNG, P.-Y. & KAWAJI, M. 2002. Investigation of two-phase flow pattern, void fraction and

pressure drop in a microchannel. *International journal of multiphase flow,* 28**,** 1411-1435.

KOHL, M., ABDEL-KHALIK, S., JETER, S. & SADOWSKI, D. 2005. An experimental investigation of microchannel flow with internal pressure measurements. *International journal of heat and mass transfer,* 48**,** 1518-1533.

KÖNIG, K. & OSTENDORF, A. 2015. *Optically induced nanostructures: biomedical and technical applications,* Walter de Gruyter GmbH & Co KG.

LAI, K., TAN, C., ONG, K. & NG, K. Thermal field simulation of multi package LED module. Next-Generation Electronics (ISNE), 2015 International Symposium on, 2015. IEEE, 1-3.

LEE, H. J. & LEE, S. Y. 2001. Heat transfer correlation for boiling flows in small rectangular horizontal channels with low aspect ratios. *International Journal of Multiphase Flow,* 27**,** 2043-2062.

LEE, P.-S. & GARIMELLA, S. V. 2006. Thermally developing flow and heat transfer in rectangular microchannels of different aspect ratios. *international journal of heat and mass transfer,* 49**,** 3060-3067.

LEE, P.-S., GARIMELLA, S. V. & LIU, D. 2005. Investigation of heat transfer in rectangular microchannels. *International Journal of Heat and Mass Transfer,* 48**,** 1688-1704.

LENG, C., WANG, X.-D., YAN, W.-M. & WANG, T.-H. 2016. Heat transfer enhancement of microchannel heat sink using transcritical carbon dioxide as the coolant. *Energy Conversion and Management,* 110**,** 154-164.

LI, H. & OLSEN, M. G. 2006a. Aspect ratio effects on turbulent and transitional flow in rectangular microchannels as measured with microPIV. *Journal of fluids engineering,* 128**,** 305-315.

LI, H. & OLSEN, M. G. 2006b. MicroPIV measurements of turbulent flow in square microchannels with hydraulic diameters from 200 μm to 640 μm. *International journal of heat and fluid flow,* 27**,** 123-134.

LI, J., PETERSON, G. & CHENG, P. 2004. Three-dimensional analysis of heat transfer in a micro-heat sink with single phase flow. *International Journal of Heat and Mass Transfer,* 47**,** 4215-4231.

LI, Y., ZHANG, F., SUNDEN, B. & XIE, G. 2014. Laminar thermal performance of microchannel heat sinks with constructal vertical Y-shaped bifurcation plates. *Applied Thermal Engineering,* 73**,** 185-195.

LIN, D. T., KANG, C.-H. & CHEN, S.-C. 2018. Optimization of the Micro Channel Heat Sink by Combing Genetic Algorithm with the Finite Element Method. *Inventions,* 3**,** 32.

LIU, C., TENG, J.-T., CHU, J.-C., CHIU, Y.-L., HUANG, S., JIN, S., DANG, T., GREIF, R. & PAN, H.-H. 2011. Experimental investigations on liquid flow and heat transfer in rectangular microchannel with longitudinal vortex generators. *International Journal of Heat and Mass Transfer,* 54**,** 3069-3080.

LIU, D. & GARIMELLA, S. V. 2004. Investigation of liquid flow in microchannels. *Journal of Thermophysics and heat transfer,* 18**,** 65-72.

MALA, G. M. & LI, D. 1999. Flow characteristics of water in microtubes. *International journal of heat and fluid flow,* 20**,** 142-148.

MISHIMA, K. & HIBIKI, T. 1996. Some characteristics of air-water two-phase flow in small diameter vertical tubes. *International journal of multiphase flow,* 22**,** 703-712.

MOHAMMED, H., GUNNASEGARAN, P. & SHUAIB, N. 2011a. Influence of channel shape on the thermal and hydraulic performance of microchannel heat sink. *International Communications in Heat and Mass Transfer,* 38**,** 474-480.

MOHAMMED, H., GUNNASEGARAN, P. & SHUAIB, N. 2011b. Numerical simulation of heat transfer enhancement in wavy microchannel heat sink. *International Communications in Heat and Mass Transfer,* 38**,** 63-68.

MUDAWAR, I. 2001. Assessment of high-heat-flux thermal management schemes. *IEEE Transactions on Components and Packaging Technologies,* 24**,** 122-141.

ONG, K., HAW, P., LAI, K. & TAN, K. Vapor chamber with hollow condenser tube heat sink. AIP Conference Proceedings, 2017a. AIP Publishing, 020018.

ONG, K., TAN, C., LAI, K. & TAN, K. 2017b. Heat spreading and heat transfer coefficient with fin heat sink. *Applied Thermal Engineering,* 112**,** 1638-1647.

ONG, K., TAN, C., LAI, K., TAN, K. & SINGH, R. Thermal management of LED with vapor chamber and thermoelectric cooling. Electronics Manufacturing Technology (IEMT) & 18th Electronics Materials and Packaging (EMAP) Conference, 2016 IEEE 37th International, 2016. IEEE, 1-7.

ONG, K. S., TAN, C. F. & LAI, K. C. 2017c. Methodological Considerations of Using Thermoelectrics with Fin Heat Sinks for Cooling Applications. *Applied Sciences,* 7**,** 62.

PATANKAR, S. V. 1980. Numerical Heat Transfer and Fluid Flow (Hemisphere, New York, 1980). *Google Scholar***,** 41-135.

PEIYI, W. & LITTLE, W. 1983. Measurement of friction factors for the flow of gases in very fine channels used for microminiature Joule-Thomson refrigerators. *Cryogenics,* 23**,** 273-277.

PENG, X. & PETERSON, G. 1995. The effect of thermofluid and geometrical parameters on convection of liquids through rectangular microchannels. *International Journal of Heat and Mass Transfer,* 38**,** 755-758.

PENG, X., PETERSON, G. & WANG, B. 1994. Heat transfer characteristics of water flowing through microchannels. *Experimental Heat Transfer An International Journal,* 7**,** 265-283.

PHILLIPS, R. J. 1987. *Forced-convection, liquid-cooled, microchannel heat sinks.* Massachusetts Institute of Technology.

PHILLIPS, R. J. 1990. Microchannel heat sinks. *Advances in Thermal Modeling of Electronic Components*.

QU, W. & MUDAWAR, I. 2002a. Analysis of three-dimensional heat transfer in micro-channel heat sinks. *International Journal of heat and mass transfer,* 45**,** 3973-3985.

QU, W. & MUDAWAR, I. 2002b. Experimental and numerical study of pressure drop and heat transfer in a single-phase micro-channel heat sink. *International Journal of Heat and Mass Transfer,* 45**,** 2549-2565.

QU, W. & MUDAWAR, I. 2003a. Flow boiling heat transfer in two-phase micro-channel heat sinks—I. Experimental investigation and assessment of correlation methods. *International journal of heat and mass transfer,* 46**,** 2755-2771.

QU, W. & MUDAWAR, I. 2003b. Flow boiling heat transfer in two-phase micro-channel heat sinks—II. Annular two-phase flow model. *International Journal of Heat and Mass Transfer,* 46**,** 2773-2784.

RAHIMI-GORJI, M., POURMEHRAN, O., HATAMI, M. & GANJI, D. 2015. Statistical optimization of microchannel heat sink (MCHS) geometry cooled by different nanofluids using RSM analysis. *The European Physical Journal Plus,* 130**,** 22.

RAHMAN, M. & GUI, F. Design, fabrication, and testing of microchannel heat sinks for aircraft avionics cooling. INTERSOCIETY ENERGY CONVERSION ENGINEERING CONFERENCE, 1993a. AMERICAN NUCLEAR SOCIETY, 1.1-1.1.

RAHMAN, M. M. & GUI, F. Experimental measurements of fluid flow and heat transfer in microchannel cooling passages in a chip substrate. The ASME International Electronics Packaging Conference, 1993b. 685-692.

RAMOS-ALVARADO, B., LI, P., LIU, H. & HERNANDEZ-GUERRERO, A. 2011. CFD study of liquid-cooled heat sinks with microchannel flow field configurations for electronics, fuel cells, and concentrated solar cells. *Applied Thermal Engineering,* 31**,** 2494-2507.

ROSS, P. E. 2004. Beat the heat. *IEEE Spectrum,* 41**,** 38-43.

SAHAR, A. M., WISSINK, J., MAHMOUD, M. M., KARAYIANNIS, T. G. & ISHAK, M. S. A. 2017. Effect of hydraulic diameter and aspect ratio on single phase flow and heat transfer in a rectangular microchannel. *Applied Thermal Engineering,* 115**,** 793-814.

SHAH, R. K. & LONDON, A. L. 1978. *Lanimar flow forced convection in duts: a source book for compact heat exchanger analytical data*, Academic press.

SHEN, H., WANG, C.-C. & XIE, G. 2018. A parametric study on thermal performance of microchannel heat sinks with internally vertical bifurcations in laminar liquid flow. *International Journal of Heat and Mass Transfer*, 117**,** 487-497.

SIDDHESHWAR, P. & VEENA, B. 2018. A Theoretical Study of Natural Convection of Water-Based Nanoliquids in Low-Porosity Enclosures Using Single-Phase Model. *Journal of Nanofluids,* 7**,** 163-174.

STANLEY, R. S., AMEEL, T. A. & BARRON, R. F. 1997. Two-phase flow in microchannels. LOUISIANA TECH UNIV RUSTON DEPT OF INDUSTRIAL ENGINEERING.

STEINKE, M. E. & KANDLIKAR, S. G. 2004. An experimental investigation of flow boiling characteristics of water in parallel microchannels. *Journal of Heat Transfer,* 126**,** 518-526.

STEINKE, M. E. & KANDLIKAR, S. G. Single-phase liquid friction factors in microchannels. ASME 3rd International Conference on Microchannels and Minichannels, 2005. American Society of Mechanical Engineers, 291-302.

SUI, Y., TEO, C., LEE, P. S., CHEW, Y. & SHU, C. 2010. Fluid flow and heat transfer in wavy microchannels. *International Journal of Heat and Mass Transfer*, 53**,** 2760-2772.

TOKIT, E. M., MOHAMMED, H. & YUSOFF, M. 2012. Thermal performance of optimized interrupted microchannel heat sink (IMCHS) using nanofluids. *International Communications in Heat and Mass Transfer*, 39**,** 1595-1604.

TRAN, T., WAMBSGANSS, M. & FRANCE, D. 1996. Small circular-and rectangular-channel boiling with two refrigerants. *International Journal of Multiphase Flow*, 22**,** 485-498.

TU, X. & HRNJAK, P. Experimental investigation of single-phase flow pressure drop through rectangular microchannels. ASME 2003 1st International Conference on Microchannels and Minichannels, 2003. American Society of Mechanical Engineers, 257-267.

TUCKERMAN, D. B. & PEASE, R. 1981a. High-performance heat sinking for VLSI. *IEEE Electron device letters*, 2**,** 126-129.

TUCKERMAN, D. B. & PEASE, R. F. W. 1981b. High-performance heat sinking for VLSI. *IEEE Electron device letters*, 2**,** 126-129.

WAMBSGANSS, M., FRANCE, D., JENDRZEJCZYK, J. & TRAN, T. 1993. Boiling heat transfer in a horizontal small-diameter tube. *Journal of Heat Transfer*, 115**,** 963-972.

WANG, G.-L., YANG, D.-W., WANG, Y., NIU, D., ZHAO, X.-L. & DING, G.-F. 2015. Heat transfer and friction characteristics of the microfluidic heat sink with variously-shaped ribs for chip cooling. *Sensors*, 15**,** 9547-9562.

WEI, X. & JOSHI, Y. 2004. Stacked microchannel heat sinks for liquid cooling of microelectronic components. *Journal of Electronic Packaging*, 126**,** 60-66.

WU, H. & CHENG, P. 2003. Friction factors in smooth trapezoidal silicon microchannels with different aspect ratios. *International journal of heat and mass transfer*, 46**,** 2519-2525.

XIE, G., LI, S., SUNDEN, B. & ZHANG, W. 2014. Computational fluid dynamics for thermal performance of a water-cooled minichannel heat sink with different chip arrangements. *International Journal of Numerical Methods for Heat & Fluid Flow*, 24**,** 797-810.

XIE, G., SHEN, H. & WANG, C.-C. 2015. Parametric study on thermal performance of microchannel heat sinks with

internal vertical Y-shaped bifurcations. *International journal of heat and mass transfer,* 90**,** 948-958.

YADAV, V., BAGHEL, K., KUMAR, R. & KADAM, S. 2016. Numerical investigation of heat transfer in extended surface microchannels. *International Journal of Heat and Mass Transfer,* 93**,** 612-622.

YIN, S., TSENG, K. J. & ZHAO, J. 2013. Design of AlN-based micro-channel heat sink in direct bond copper for power electronics packaging. *Applied Thermal Engineering,* 52**,** 120-129.

ZHANG, C., CHEN, Y. & SHI, M. 2010. Effects of roughness elements on laminar flow and heat transfer in microchannels. *Chemical Engineering and Processing: Process Intensification*, 49**,** 1188-1192.

ZHANG, H., PINJALA, D., JOSHI, Y., WONG, T., TOH, K. & IYER, M. Fluid flow and heat transfer characteristics of liquid cooled foam heat sinks. Thermal and Thermomechanical Phenomena in Electronic Systems, 2004. ITHERM'04. The Ninth Intersociety Conference on, 2004. IEEE, 640-647.

ZHANG, H., PINJALA, D., WONG, T., TOH, K. & JOSHI, Y. 2005. Single-phase liquid cooled microchannel heat sink for electronic packages. *Applied Thermal Engineering,* 25**,** 1472-1487.

ZHANG, L., KOO, J.-M., JIANG, L., ASHEGHI, M., GOODSON, K. E., SANTIAGO, J. G. & KENNY, T. W. 2002. Measurements and modeling of two-phase flow in microchannels with nearly constant heat flux boundary conditions. *Journal of Microelectromechanical systems*, 11**,** 12-19.

PUBLICATIONS

No	Title
1	Wei Long, Y., Kim Ho, Y., Koon Chun, L., Pei Song, C., & Kok Seng,O. (2018). Effect of Microfins on Thermal Performance of Microchannel Using CFD. International Journal of Engineering & Technology, 7(3.14), 1-4. DOI: 10.14419/ijet.v7i3.14.16852. (Published)
2	Yeo, W.L., Yeap, K.H., Lai, K.C., Ong, K.S. and Chee, P.S., 2018. Numerical Study on Heat Transfer in a Microchannel with Micro-fins. Applications of Modelling and Simulation, 2(3), pp.102-106. (Published)
3	Yeo, W.L., Yeap, K.H., Lai, K.C., Ong, K.S. and Chee, P.S., 2018. Numerical And Experimental Investigation Of Microchannel Heat Sink With Micro-Fins. Jurnal Fizik Malaysia (JFM), 39(1), pp.10029-10040. (Published)

APPENDIX

APPENDIX A: Tables

Table 6.0: The simulation result of 4 thermocouples for bare rectangular microchannel

Reynolds Number (Re)	Thermocouple 1 (T_w 1) (K)	Thermocouple 2 (T_w 2) (K)	Thermocouple 3 (T_w 3) (K)	Thermocouple 4 (T_w 4) (K)	Average Temperature (K)
400	346.932	351.636	355.585	357.941	353.0235
600	342.045	347.019	350.71	352.0932	347.9668
800	340.994	344.95	349	348.944	345.972
1000	339.963	343.416	345.82	346.855	344.0135
1200	339.975	342	343.937	345.9401	342.963

Table 6.1: The experiment result of 4 thermocouples for bare rectangular microchannel

Reynolds Number (Re)	Thermocouple 1 (T_w 1) (K)	Thermocouple 2 (T_w 2) (K)	Thermocouple 3 (T_w 3) (K)	Thermocouple 4 (T_w 4) (K)	Average Temperature (K)
400	342.5	345	349	352	347.125
600	340	343	345.4	346.5	343.725
800	339	341	343	344	341.75
1000	338	339	341.1	342	340.025
1200	337	338.2	340	341	339.05

Table 6.2: The simulation result of 4 thermocouples for rectangular microchannel with micro-fins

Reynolds Number (Re)	Thermocouple 1 (T_w 1) (K)	Thermocouple 2 (T_w 2) (K)	Thermocouple 3 (T_w 3) (K)	Thermocouple 4 (T_w 4) (K)	Average Temperature (K)
400	340.023	345.11	349	354.029	347.0405
600	337.519	340.195	343.074	347.224	342.003
800	336.109	339.436	341.356	343.403	340.076
1000	334.096	337.183	339.022	342.0195	338.0801
1200	333.445	336.313	338.142	340.126	337.0065

Table 6.3: The experiment result of 4 thermocouples for rectangular microchannel with micro-fins

Reynolds Number (Re)	Thermocouple 1 (T_w 1) (K)	Thermocouple 2 (T_w 2) (K)	Thermocouple 3 (T_w 3) (K)	Thermocouple 4 (T_w 4) (K)	Average Temperature (K)
400	335	337.9	342	345	339.975
600	332.5	336	338.5	341	337
800	330.5	334.6	337	338	335.025
1000	330	333	336	337.1	334.025
1200	330	332.5	335.4	337	333.725